universität wien

MASTERARBEIT / MASTER'S THESIS

Titel der Masterarbeit / Title of the Master's Thesis

"Generation of Nanoplastic Aerosols from Polyethylene (PE), Polypropylene (PP), and Polyethylene Terephthalate (PET) Macroplastics"

verfasst von / submitted by

Andrea Stöllner, BSc

angestrebter akademischer Grad / in partial fulfilment of the requirements for the degree of

Master of Science (MSc)

Wien, 2020 / Vienna, 2020

Studienkennzahl lt. Studienblatt / degree programme code as it appears on the student record sheet:	UA 066 876
Studienrichtung lt. Studienblatt / degree programme as it appears on the student record sheet:	Masterstudium Physik
Betreut von / Supervisor:	Assoz. Prof. Dr. Paul Winkler

Abstract

Plastic pollution is one of the main environmental concerns humanity faces today. However, the problem lies not only with carelessly discarded water bottles and drinking straws. Small plastic particles in the millimeter to nanometer range gain more and more attention as a major threat to the environment and to human health. These micro- and nanoplastics make their way all around the globe and have been detected in oceans, freshwater systems, soils, and the atmosphere. Many scientists focus on microplastics in marine environments, but little is known about airborne plastic particles and their sources. This thesis aims to investigate a possible source of airborne nanoplastics by heating everyday plastic items – a polyethylene (PE) packaging foil, a polypropylene (PP) candy box, and a polyethylene terephthalate (PET) water bottle. The conditions under which these plastics produce nanoparticles by evaporation, homogeneous nucleation, and subsequent condensation of plastic vapor were investigated. Number size distributions of the generated aerosols were recorded and evaluated and comparison measurements with additive-free PE, PP, and PET were conducted. The results give a first estimate of which industrial processes and everyday activities could produce airborne nanoparticles by heating plastics and invite further investigation of nanoplastic aerosols in the context of cloud formation and the impacts of atmospheric plastic pollution on the environment and on human health.

Zusammenfassung

Umweltverschmutzung durch Plastik ist eine der größten ökologischen Hürden unserer Zeit. Doch das Problem liegt nicht nur bei unachtsam weggeworfenen Trinkflaschen und Strohhalmen. Kleine Plastikteilchen im Millimeter- bis Nanometerbereich rücken mehr und mehr in den Fokus von Wissenschaftler*innen und werden als ernstzunehmende Gefahr für die Umwelt und die menschliche Gesundheit erkannt. Diese Mikro- und Nanoplastikteilchen erreichen sogar die entlegensten Orte der Erde und wurden bereits in Ozeanen, Süßwassersystemen, Böden und der Atmosphäre nachgewiesen. Viele Wissenschaftler*innen befassen sich mit Mikroplastik in marinen Ökosystemen, doch nur wenig ist über atmosphärische Nanoplastikteilchen und deren Herkunft bekannt. Diese Arbeit beschäftigt sich mit einem möglichen Entstehungsmechanismus solcher Teilchen durch Erhitzung von Alltagsgegenständen aus Plastik – einer Verpackungsfolie aus Polyethylen (PE), eines Süßigkeitenbehälters aus Polypropylen (PP), und einer Wasserflasche aus Polyethylenterephthalat (PET). Die Bedingungen, unter denen diese Plastikarten Nanoteilchen durch Verdunstung, homogene Nukleation, und anschließende Kondensation von Plastikdampf erzeugen, wurden untersucht. Partikelgrößenverteilungen der erzeugten Aerosole wurden gemessen und charakterisiert und mit Messungen von zusatzstofffreiem PE, PP, und PET verglichen. Die Ergebnisse dieser Arbeit liefern eine erste Abschätzung, welche industriellen Verfahren und alltäglichen Tätigkeiten luftgetragene Nanoteilchen durch Erhitzung von Plastik erzeugen könnten, und bildet die Grundlage für weitere Forschung an Nanoplastikaerosolen in Bezug auf Wolkenbildung und den Einfluss von Luftverschmutzung durch Plastik auf die Umwelt und die menschliche Gesundheit.

Table of Contents

1 Introduction 7

1.1 Motivation and Background 7

1.1.1 Plastic Pollution as a Global Problem 8

1.1.2 Health Risk of Airborne Plastic Particles 9

1.1.3 Origin of Airborne Nanoplastics 10

1.2 Thesis Scope and Research Question 11

1.2.1 Approach and Methods 11

1.2.2 The Question(s) to Be Answered 12

2 Theoretical Background 13

2.1 What is Plastic? 13

2.1.1 Chemical Structure of Plastics 14

2.1.2 Chemical Additives 17

2.1.3 Degradation of Plastic 18

2.1.4 Polyethylene (PE) 19

2.1.5 Polypropylene (PP) 20

2.1.6 Polyethylene Terephthalate (PET) 21

2.2 Environmental Plastic Pollution 22

2.2.1 Pathways into the Environment 22

2.2.2 The Microplastic Cycle 23

2.2.3 Macro-, Micro- and Nanoplastics 24

2.2.4 Impacts on Environmental and Human Health 26

2.3 Relevant Concepts of Aerosol Physics 27

2.3.1 The Saturation Ratio 27

2.3.2 Homogeneous Nucleation and the Kelvin Equation 28

2.3.3 Description in Classical Nucleation Theory 29

3 Methodology and Experimental Setup 31

3.1 Preparation of PE, PP, and PET Samples 31

3.2 Experimental Setup 33
3.2.1 Tube Furnace 33
3.2.2 Aerosol Charger 34
3.2.3 Differential Mobility Analyzer (DMA) 35
3.2.4 DMA Resolution and Transfer Function 38
3.2.5 Faraday Cup Electrometer (FCE) 39
3.2.6 The Final Setup 40
3.3 Data Collection and Evaluation 41
3.4 Uncertainty Estimation 42
4 Experiment and Results 45
4.1 Sample Morphology During Heating 45
4.2 Temperature Profiles of Commodity LDPE, PP, and PET 48
4.2.1 Temperature Dependence of Maximum Particle Concentration 50
4.2.2 Temperature Dependence of Electrical Mobility Diameter 50
4.3 Number Size Distributions of Commodity Plastics 51
4.3.1 Commodity LDPE 52
4.3.2 Commodity PP 53
4.3.3 Commodity PET 54
4.4 Additive-Free Polymers Versus Commodity Plastics 55
4.5 Miscellaneous Findings and Troubleshooting 58
4.5.1 Unstable Particle Concentrations 58
4.5.2 Reusing Old Samples 59
4.5.3 Effect of Cooling Temperature After the Furnace 60
4.5.4 Plastic Contamination of the Experimental Setup 61
5 Discussion and Conclusion 63
6 Future Research 65
7 Closing Remarks 66

Acknowledgments

I would like to express my special thanks to Assoc. Prof. Dr. Paul Winkler for supervising this master's thesis and for the patience and delight for his field with which he teaches his courses. As his student, I was never afraid to ask something potentially foolish – and from that sort of question there were many. Professor Dr. Winkler always has a sympathetic ear for his students' problems and inquiries and for that I am very grateful. Secondly, I would like to thank Peter Wlasits, Sascia Kästenbauer, Paulus Bauer, Carl Trondl, and Loic Gonzalez for our time together in the lab. Thank you for the many laughs and for teaching me how to solder a cable, how to deconstruct a DMA, how to reconstruct a DMA, how to more or less safely set plastic on fire (although that is explicitly not the goal of this master's thesis) and many, many things more. Thank you for the great time together! Finally, I would like to thank my friends and family who always have my back, no matter what I set my mind to. Thank you for the many late-night discussion about anything and everything and for your steady support in my life. I could not have done this thesis (or anything, really) without you.

While doing research for this master's thesis, I came across a quote I knew I had to include in my writing. In a strange kind of way, it captures exactly what I love about the field of physics and why I chose to study it:

"Aristotle said a bunch of stuff that was wrong. Galileo and Newton fixed things up. Then Einstein broke everything again. Now, we've basically got it all worked out, except for small stuff, big stuff, hot stuff, cold stuff, fast stuff, heavy stuff, dark stuff, turbulence, and the concept of time."

— Zach Weinersmith, Science: Abridged Beyond the Point of Usefulness

There is always more to learn, more to discover, and more to find out. This thesis will in particular deal with small as well as hot stuff (although not too small or too hot). With it I hope to contribute a little bit to fixing our knowledge of science – or perhaps breaking it, whichever brings more insight.

1 Introduction

This thesis aims to make a small contribution to help understand and hopefully resolve one of the major (and sadly numerous) environmental crises of the 21st century – plastic pollution. Plastics have become ubiquitous in our everyday lives, quite literally following us everywhere we go – from water bottles and disposable coffee cups, over technical devices and the packages they come in, up to the clothes we wear and cosmetic articles we put on our skin and brush our teeth with. Thus, it is hardly surprising that plastic has made its way not only into our lives and our bodies but into practically every corner of our planet. It is in the soil we stand on, in the water we drink, and in the air we breathe. As the final project for my master's studies in the field of atmospheric aerosol physics, the latter shall be the focus of this thesis.

1.1 Motivation and Background

The wide range of properties and possible applications for plastics has reshaped our world since Bakelite – the first fully synthetical polymer – was produced by Hendrick Baekeland, just a little more than 100 years ago in 1907 [1]. Since then, countless different plastic types have been developed, each designed to meet the specific requirements of a different product or industry. Crawford and Quinn (2017) even describe plastics as "the pinnacle of technological innovation" [1]. But there is a flip side to this outstanding success story. With 359 million tons of plastics produced globally in 2018 [2], the problem of plastic pollution has over the last decade become a major focal point of the environmental protection movement, both in the eye of the public as well as in research. Depressing footage of fish, turtles, and birds caught in marine plastic debris sends a clear message of a problem that needs addressing. Perhaps precisely because of this powerful and disturbing visual imagery, plastic pollution has moved to the forefront of every environmental crisis discussion, for some maybe even more so than the pressing issue of ever-rising CO_2 emissions. The need for action seems to be clear and the first steps against plastic pollution have already been taken. Since the beginning of the year 2020, for example, Austria has banned single-use, non-biodegradable plastic bags from being sold in stores as well as the addition of microplastic particles to products from the cosmetic and cleaning agent industry [3]. Still, the problem of plastic pollution seems to many of us like a rather distant one – something that effects only oceans and rivers and impacts our personal lives only if we eat too much shellfish. Research is starting to show, that this might be a grave underestimation of the multifaceted problem at hand.

1.1.1 Plastic Pollution as a Global Problem

Plastics have found their way not only into the hydrosphere and its wildlife but also all other major parts of the earth system – the geosphere, the biosphere, and, for this thesis most importantly, the atmosphere. While bigger plastic pieces are too heavy to stay suspended in air long enough to be considered an aerosol, micro- and nanoplastics (commonly defined as being smaller than 5 mm and 1 μm, respectively) gain interest among aerosol physicists. Atmospheric deposition of microplastics has been observed in highly populated cities like Paris, France [4], Bremen, Germany [5], and Dongguan, China [6] as well as in sites far off human civilization. Microplastics have been found in a remote mountain catchment in the French Pyrenees [7], the Swiss Alps, and even the Arctic [5] – places, that until now were considered to be "pristine". These findings suggest that microplastics can be transported in the atmosphere over distances of up to 95 km [7] and possibly even considerably further. On atmospheric pathways from Europe to the Arctic, microplastics could travel distances of up to 3.500 km [5]. Consequently, atmospheric micro- and nanoplastics could influence cloud formation and therefore radiative forcing. The plastic particles could act as cloud condensation nuclei and ice nucleating behavior of polyethylene and polypropylene was already shown by Ganguly and Ariya (2019) both in freshwater and seawater in a lab setting [8]. Yet, to realistically gauge the effects of micro- and nanoplastics on cloud formation and anthropogenic climate change, more research in this field is necessary.

Figure 1 shows the nine planetary boundaries as first described by Rockström et al. (2009) [9] and later updated by Steffen et al. (2015) [10]. The green area inside the inner heavy circle is considered to be a safe operating space for humanity, while yellow and red symbolize increasing or high risk of irreversible and possibly catastrophic changes to the earth system [9]. Micro- and nanoplastics contribute to pollution by novel entities (formerly chemical pollution) and atmospheric aerosol loading. Both of these planetary boundaries have not yet been quantified on a global scale, meaning that it is not clear what amount of novel entities in the environment and aerosol loading of the atmosphere is "safe" and whether or not we have already left this safe operating space [10]. An argument can be made that micro- and nanoplastics also contribute to the threats against the planetary boundaries of biosphere integrity and climate change. As of 2016, we have already overstepped the safe operating space for both genetic biodiversity loss and climate change [10].

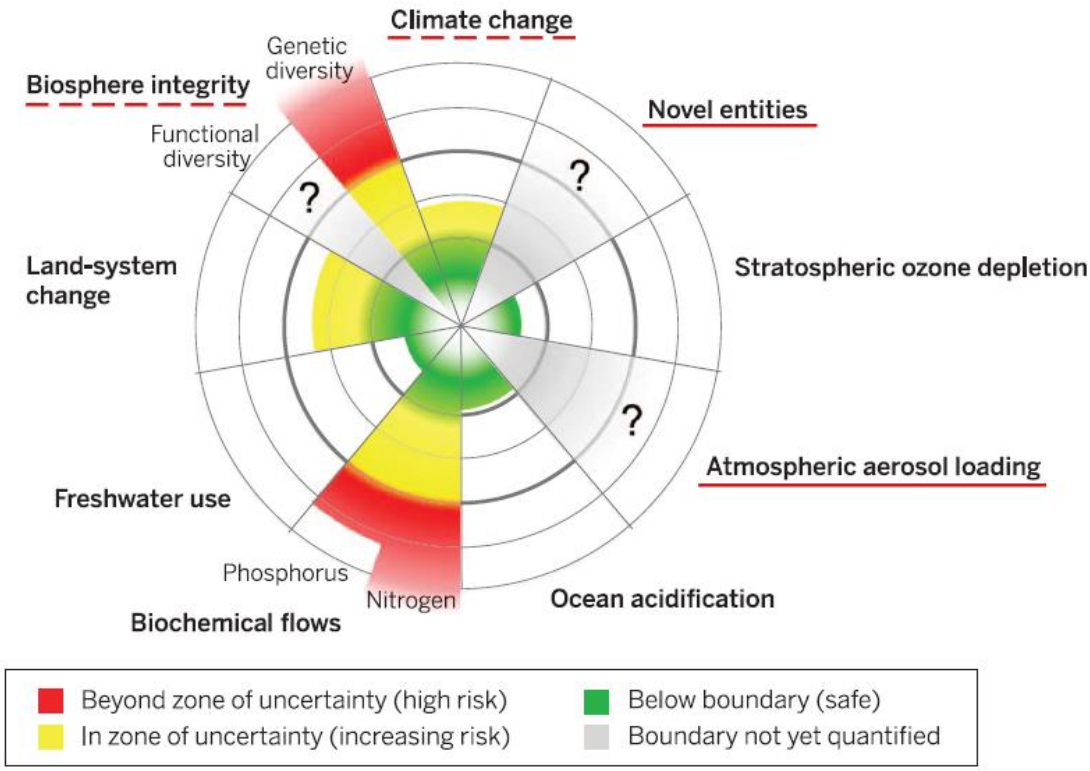

Figure 1: The nine planetary boundaries. Micro- and nanoplastics contribute directly to atmospheric aerosol loading and pollution by novel entities (red underline) and indirectly to the threats against the planetary boundaries for biosphere integrity and climate change (dashed underline). Adapted from Steffen et al., 2015 [10].

1.1.2 Health Risk of Airborne Plastic Particles

Atmospheric pollution by plastic particles is not only posing a threat to the environment but also to human health. While numerous studies on microplastics and their environmental risks are ready to be found, less research is done about nanoplastics. On one hand, this is because of a higher methodological difficulty [11], on the other hand, because a clear, widely accepted distinction between micro- and nanoplastics is still missing. Many papers on atmospheric plastic pollution do not distinguish between the two particle sizes at all or do not consider particles below a certain threshold, leaving nanoplastic mostly uninvestigated. In adverse contrast to that, the papers that do concern themselves with nanoplastics specifically, suggest that the smaller particles pose a greater risk than microplastics. This is because of the much higher environmental exposure from nanoplastics compared to microplastics [11], as well as the fact that some nanoplastic particles are small enough to enter cellular tissue [12]. Developing zebrafish exposed to polystyrene nanoparticles were shown to accumulate nanoplastics in various organs such as the gallbladder, liver, pancreas, heart, and brain [13].

Similar effects could also be possible in humans, given a high enough exposure. Micro- and nanoparticles can enter the human body on three main pathways – through ingestion via the gastrointestinal tract, respiration via the lungs, or uptake via the skin [14]. In terms of aerosol physics, the uptake of airborne micro- and nanoplastics through the lungs is most interesting and some research on the topic has already been done. Industrial workers who are exposed to chronically high concentrations of airborne microplastics due to their field of work show a variety of respiratory occupational diseases such as shortness of breath, cough, chronic bronchitis, impaired lung function or increased risk of lung cancer [15]. It is yet to be determined, if lower environmental concentrations could have similar effects on human health.

1.1.3 Origin of Airborne Nanoplastics

Micro- and nanoplastics are classified into primary and secondary particles according to their origin. Primary micro- and nanoplastics are directly emitted to the environment. They are produced as microbeads for the use in cosmetic products and cleaning agents or as raw material to manufacture other plastic products. Costa (2018) also lists fibers released during washing and drying of clothing as primary plastic particles, although they are not intentionally produced. By contrast, secondary microplastics form unintentionally via the breakdown of larger plastic debris – also called macroplastics – that is already in the environment, like plastic bottles, bags, fishing nets, etc. Subsequently, secondary nanoplastics form due to the breakdown of microplastics [16]. The mechanisms by which larger plastics break down into smaller particles range from thermal and mechanical degradation over photo- and atmospheric oxidation up to decomposition by bacteria, fungi, or animals [1]. While the general production and degradation processes of primary and secondary micro- and nanoplastics are well understood, there is little research yet to be found about their concrete sources and pathways into the environment. The majority of papers on the topic concentrates on microplastics in marine or freshwater ecosystems [17]. For the case of airborne micro- and nanoplastics, there is little to no peer-reviewed information available, although some suggestions and hypotheses are made. Gasperi et al. (2018) for example propose industrial processing of synthetic materials or environmental degradation in combination with wind shear or abrasion as possible sources for airborne micro- and nanoplastics [17]. Dris et al. (2016) mention synthetic fibers from clothing and houses as well as landfills or waste incineration as possible sources but find that "More work is needed in order to investigate these atmospheric fibers and understand where they come from, where they end up and which mechanisms and factors lead to their transport and their fallout."

1.2 Thesis Scope and Research Question

As discussed above, micro- and nanoplastics are present in the atmosphere, but little is known about where they come from and how they get there. Although some possible sources of airborne plastic particles are mentioned in literature, tangible research on the topic is missing. To help take a first step in the direction of concrete evidence on the sources of nanoplastics in the atmosphere, this thesis concerns itself with nanoplastic formation from plastic vapor.

1.2.1 Approach and Methods

In this experiment, it was investigated if a nanoparticle aerosol can be formed by heating different kinds of commonly used plastics in a tube furnace and by cooling the formed vapor to induce homogeneous nucleation and condensation of nanoparticles. This approach has been described by Scheibel and Porstendörfer in 1983, who used this method to generate monodisperse Ag- and NaCl-aerosols in the size range of 2 to 300 nm [18]. In accordance with this method of generation, only aerosol particles in the nano range were investigated. A strict definition of the different size ranges of plastic particles, especially nanoplastics, is given in chapter 2.2.3 “Macro-, Micro- and Nanoplastics”. The nanoparticle aerosols were measured using a Differential Mobility Particle Sizer (DMPS) setup consisting of a University of Vienna-type nano Differential Mobility Analyzer (nano-DMA) and a Faraday Cup Electrometer (FCE). The goal was to obtain size distributions of the generated aerosols using different plastic types and furnace temperatures. A more in-depth discussion of the techniques and instruments mentioned above can be found in chapter 3 “Methodology and Experimental Setup”.

1.2.2 The Question(s) to Be Answered

The main research question of this thesis is: “Is it possible to generate a nanoparticle aerosol by homogeneous nucleation and subsequent condensation of plastic vapor, produced by heating PE, PP, and PET macroplastics?” or more loosely formulated:

“Can airborne nanoparticles be generated by heating plastic?”

If so, the heating of plastics would be a possible source of airborne nanoparticles and could help understand the pathways on which nanoplastics reach the atmosphere and are distributed in the environment. The size distributions of the generated aerosols were characterized by their maximum concentrations, particle diameters, and distribution widths. Possible dependencies on plastic type (here PE, PP, and PET) and heating temperatures were investigated.

The size distribution of a given aerosol is a relevant factor in determining the health risk posed by the aerosol particles entering the body, as smaller particles can enter cellular tissue or even penetrate cell membranes as discussed in chapter 2.2.4 “Impacts on Environmental and Human Health”. A comparison between different kinds of plastic is of special interest, as not only size but also chemical composition is a relevant factor in an environmental and human health risk assessment (among other characteristics like surface structure or particle shape). Polyethylene (PE), polypropylene (PP), and polyethylene terephthalate (PET) were chosen for this comparison, as they are the three main contributors to today’s global plastic waste. A chemical description of the investigated plastic types, as well as a breakdown of the different percentages with which they contribute to global plastic waste, can be found in chapter 2 “Theoretical Background”.

Finally, the temperatures at which nanoparticle aerosols are generated from heated plastic give a first idea of where this mechanism could be happening in the field. Nanoplastic aerosol release from human activities such as cooking or cleaning or from plastics that are already in the environment and get heated by the sun could be thinkable. At the higher end of the temperature scale to which plastics are commonly exposed to lie waste incineration plants that must reach temperatures of at least 850 °C for two seconds in accordance with the European Waste Incineration Directive [19].

2 Theoretical Background

While the primary research question of this thesis “Can airborne nanoparticles be generated by heating plastic?” is a quite simple yes or no question that was answered within the very first day of measurement, the science behind it is highly interesting and quite encompassing. To truly understand the question, its implications, and the importance of asking it, requires some theoretical background from a few scientific fields – including materials physics, chemistry, environmental science, and of course aerosol physics. The following paragraphs aim to give this background. The chapter starts with a close look at what exactly plastic is and continues with plastic’s way into and impact on the environment. The closing pages of this section deal with the concepts of aerosol physics necessary to conduct and understand the methodology of this experiment.

2.1 What is Plastic?

The defining characteristic of any plastic material is to be found in its molecular structure. Individual molecules, so-called monomers, are linked together to form polymer chains in a process called polymerization. The properties of the formed plastic depend on the composition of these polymer chains, as well as their interaction with one another in the form of possible crystallinity or branching [1]. Plastic materials are usually classified into the two groups of thermoplastic and thermosetting polymers with the latter at times being divided further into duroplasts and elastomers. The three plastic types examined in this experiment, polyethylene (PE), polypropylene (PP), and polyethylene terephthalate (PET) are all thermoplastics, meaning they soften reversibly upon heating and harden out upon cooling. They can exhibit a degree of crystallinity and therefore have a defined melting temperature. In contrast to that, thermosets do not soften when heated and degrade before they reach their melting temperature [20]. The following paragraphs give a short introduction into the structure of plastics in general as well as the specific properties of PE, PP, and PET. The end of the chapter deals with the thermal-oxidative degradation of plastic as the most relevant plastic degradation process with regards to this experiment.

2.1.1 Chemical Structure of Plastics

A plastic material's properties like ductility, strength, melting point, optical features, or resistance to chemicals are determined by the characteristics of the polymer chains forming the plastic. They depend on the chain's length, the monomer composition, the stereochemistry (the spatial arrangement of the monomers), polymer crystallinity, and branching of the different polymer chains. **Figure 2** shows the chemical structure of polypropylene. The monomer forming the polymer chain is called propene (also called propylene) with the chemical formula C_3H_6. The polymer chain, which consists of around 10^4 to 10^8 monomers for commercial plastics, is formed by polymerization of the propene monomers and can (in the case of polypropylene) be isotactic, syndiotactic, or amorphous. The chain pictured in **Figure 2** is syndiotactic, meaning that the CH_3 groups are configured in an alternating but regular arrangement with one showing "up", the next "down", and so on.

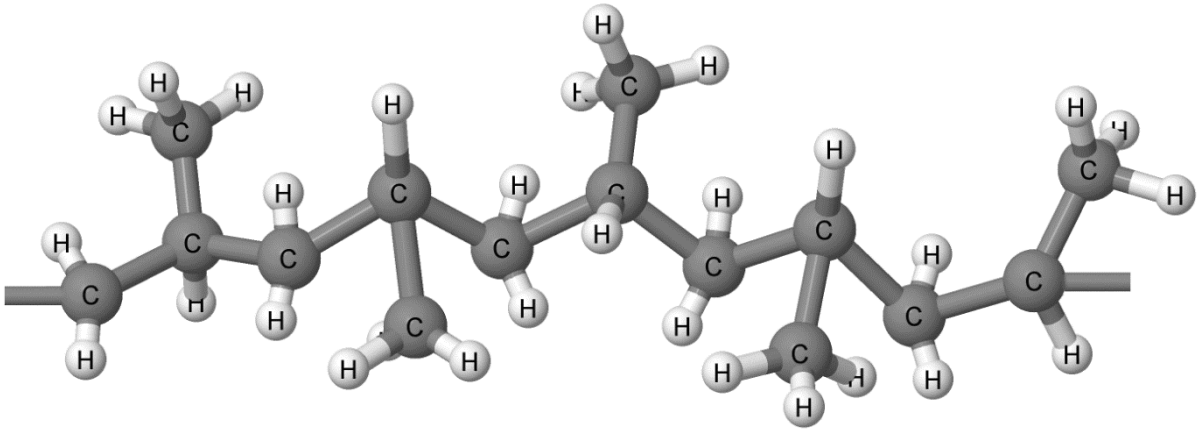

Figure 2: Polymer chain of syndiotactic polypropylene. Illustration created with Jmol [52].

In isotactic polymer chains, the asymmetric carbon groups are arranged identically, showing in the same direction, while for atactic polypropylene the monomers are stereorandom and show no configurational regularity. Whether or not a given polymer has such distinct stereochemical variants depends on the symmetry of its synthesizing monomer. Those that do, such as polypropylene, show that tacticity directly affects the physical properties of the formed plastic. According to Crawford and Quinn (2017) isotactic polypropylene is rigid with a melting point of around 160 °C, while syndiotactic polypropylene is more ductile with a melting point of 130 °C. Atactic polypropylene does not have a specific melting point and exhibits rubber-like properties. Polyethylene and polyethylene terephthalate do not have stereochemical variants [1].

2.1.1.1 Crystallinity, Branching, and Crosslinking

Not only the individual polymer chains themselves affect the properties of a given plastic material but also how they are arranged with respect to each other. While atactic polymer chains only form amorphous plastics, the two stereoregular variants can form polymer crystallites. In these crystalline regions, the polymer chains are aligned to form lamellae [1]. **Figure 3** shows a crystalline region in isotactic polypropylene with the lamellae forming a petal-like shape, resembling a flower. The image was taken using atomic force microscopy by Zhang et al. (2017) [21]. Depending on the type of semi-crystalline plastic, 10 % to 80 % of the polymer chains are in ordered crystalline structures while the rest is amorphous. Plastics with a higher degree of crystallinity exhibit higher strength and resistance to chemicals as well as a higher and more distinct melting point, while amorphous thermoplastics have no clear melting point but simply become softer and softer upon heating. Furthermore, amorphous regions appear transparent, while semi-crystalline regions are translucent [1]. With all three examined plastic types PE, (commercially available) PP, and PET being semi-crystalline thermoplastics, this change in appearance was also observed during this experiment while heating and cooling the plastics, which induces a phase transition from a semi-crystalline solid phase to an amorphous liquid phase and back. Images of the plastics' appearances before and after heating can be found in the results section of this thesis.

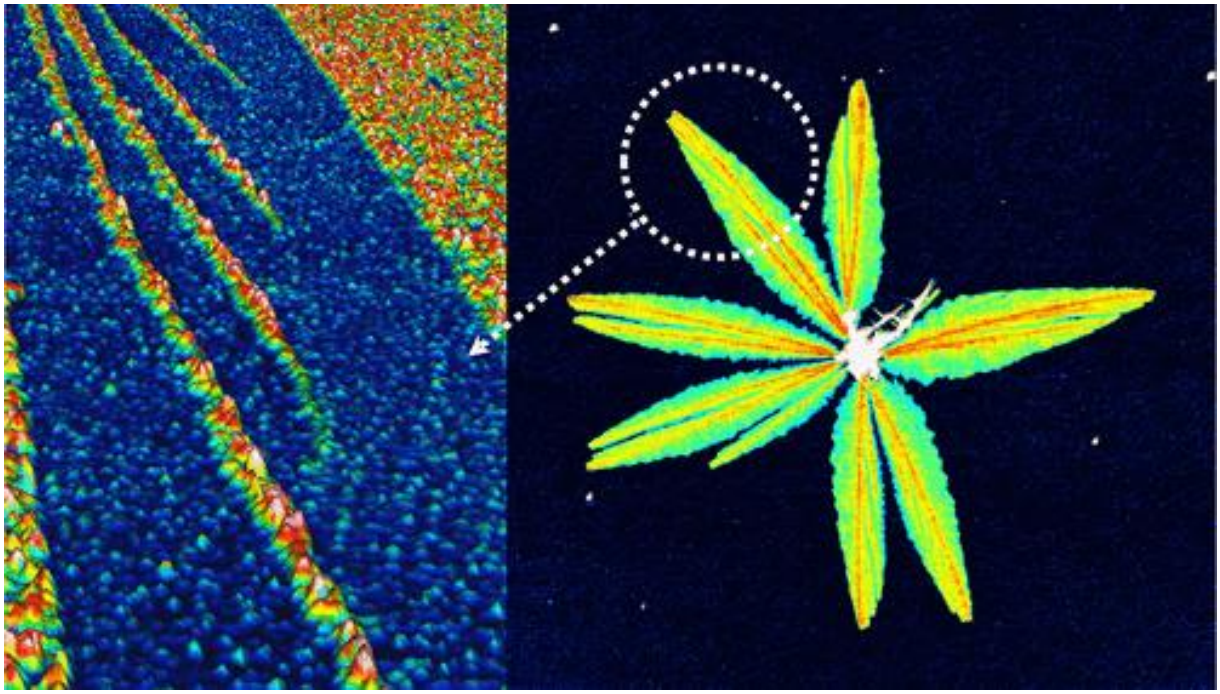

Figure 3: Atomic force microscopy image of an isotactic polypropylene crystal. The left side shows a magnification of the petal-like lamellae shown on the right side. Illustration by Zhang et al., 2017 [21].

Another way in which polymer chains interact with each other inside a plastic material is by forming branches. A branched polymer consists of main polymer chains to which several smaller polymer chains are attached. A higher number of branches leads to larger space in-between main polymer chains, thus lowering density and increasing flexibility [1]. Branching also influences the material's melting temperature and glass transition temperature, as discussed in the following paragraph. Branching is not to be confused with crosslinking, in which main polymer chains are connected with each other. The distinct properties of thermosets mentioned above (for example that they do not soften upon heating) are a result of the strong covalent bonds of crosslinking [22].

2.1.1.2 Glass Transition Temperature and Melting Temperature

It is useful to introduce two different temperature points to describe the properties of a polymer – one being the glass transition temperature and one being its melting temperature. These two temperatures depend on the chemical structure of the polymer as described above, as well as the plastic's degree of crystallinity, branching, and crosslinking. The glass transition temperature T_g is defined as the temperature above which the material becomes soft or rubbery as the polymer chains start to noticeably slide past each other. Below T_g, the polymer chains do not have enough thermal energy to move around and the plastic is brittle and rigid, resembling glass. Plastics with a glass transition temperature below the temperature at which they are typically used (for commodity plastics like packaging and water bottles this is usually room temperature) are pliable and easy to deform [20]. An example of this is plastic bags made from low-density polyethylene, which has a glass transition temperature of T_g = - 110 °C [1]. The glass transition temperature is a characteristic of amorphous polymers. As most plastics are at least partially amorphous, most plastics have a glass transition temperature. By contrast, a distinct melting temperature T_m is a characteristic of semi-crystalline polymers. Thus, only plastics with a non-neglectable degree of crystallinity have a melting point, whereas wholly amorphous polymers gradually soften when heated or stay unaltered until they reach a high enough temperature to induce thermal-oxidative degradation [20]. **Figure 4** depicts a material's stiffness in relation to its temperature. Amorphous materials become softer after reaching their T_g, while semi-crystalline materials remain mostly unaltered until they reach their melting point T_m.

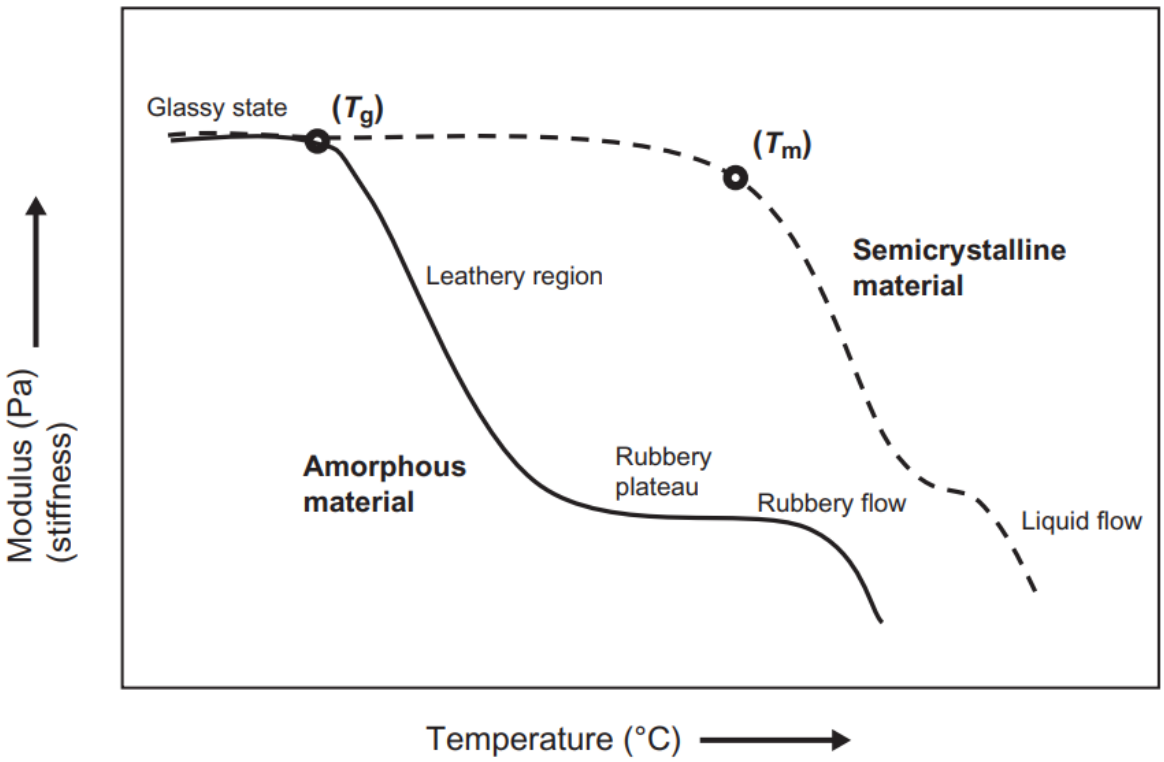

Figure 4: Softening behavior of amorphous and semi-crystalline materials upon heating. Illustration by Shrivastava, 2018 [20].

2.1.2 Chemical Additives

Besides polymer chains, which define a plastic material's general properties, most commercial plastics contain chemical additives. They are added to alter the polymer's properties or to make it more resistant to degradation, both during processing and during use. Common plastic additives include plasticizers, colorants, antistatics, heat-, light-, and oxidative stabilizers, flame retardants, surface modifiers, etc. [1]. The topic of chemical additives is especially relevant to this thesis. Without a chemical or mass spectrometric analysis, it cannot be known whether the aerosol particles generated from everyday plastic items are polymer chain fragments and thus nanoplastics or simply evaporating additives. The loss of additives from plastics is a known problem that impairs mechanical performance over time and is a possible contamination source of packaged food, bottled water, air, and the environment in general. Wei et al. (2019) have shown that plasticizers diffuse to a polymer surface from which they evaporate to a surrounding gas phase at elevated temperatures. If the plasticizers diffuse faster than they can evaporate, a plasticizer film can form on the surface [23]. This so-called evaporation-controlled additive loss has likely also happened during this experiment in the case

of polyethylene. A more in-depth discussion of this effect and how it was observed during the experiment can be found in chapter 4 “Experiment and Results”. If evaporation is faster than the diffusion rate to the surface, the additive loss is diffusion-controlled, leading to an additive gradient within the material [23].

2.1.3 Degradation of Plastic

Plastic degrades when its polymer chains break into smaller pieces in a mechanism called chain scission. In biotic degradation, the polymer chains are degraded by biological organisms like bacteria, fungi, worms, or insects. Besides this biotic degradation, there are different modes of abiotic degradation: Mechanical, photo-oxidative, chemical, degradation by gases (e.g. in the atmosphere), by water (e.g. in the ocean), and – for this thesis most importantly – by heat. The latter is called thermal degradation, in the presence of oxygen also thermal-oxidative degradation, and occurs when plastic reaches its degradation temperature. At this degradation temperature, the thermal energy is high enough to overcome the energy barrier for the breakdown of polymer chains and the plastic degrades. In a process called “polymer free radical chain reaction”, highly reactive, free radicals are formed by the breakdown of the polymer chain which subsequently react with oxygen to form other radical molecules. These in turn react with oxygen themselves and create more free radicals, breaking the polymer chain further and further. This goes on until there is not enough oxygen or heat to continue the process [1]. At which temperature this thermal-oxidative degradation becomes relevant depends on the molecular structure of the polymer and environmental conditions such as UV exposure and the amount of available oxygen. Additives also influence the degradation temperature with some of them specifically designed to increase thermal and oxidative stability. To measure degradation temperatures, a technique called thermogravimetric (TG) analysis is used. In TG analysis, the sample is continuously heated and its change in mass is recorded. Mass loss is a clear indication of degradation, although some degradation can also happen before a significant mass loss occurs [24]. Sudip and Cooney (2018) measured the thermal-oxidative degradation temperatures of PE, PP, and PET in air, using thermogravimetric analysis. Mass loss of PE and PP was observed from 250 °C upwards with PP showing lower thermal stability, decomposing significantly faster than PE. For PET in air, a decomposition onset temperature of 350 °C was found [24].

2.1.4 Polyethylene (PE)

Chemical formula	$(C_2H_4)_n$
Monomer name	Ethene (aka ethylene)
Glass transition temperature	- 110 °C
Melting temperature	116 °C (LDPE) 125 °C to 140 °C (HDPE)
Degradation temperature	250 °C
Share of global plastic waste	34 %
Common applications	Plastic bags, food packaging, toys, shampoo bottles, garden furniture, etc.

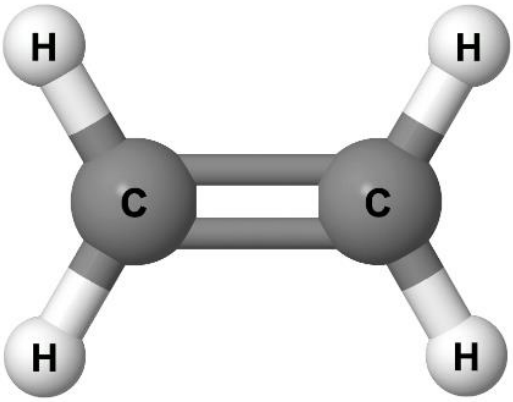

Figure 5: Ethene monomer. Illustration created with Jmol [52].

Polyethylene (PE) is the most produced and most discarded of all plastic types. 30 % of plastic produced in Europe in 2018 [2] and 34 % of global plastic waste in 2015 [25] was polyethylene. Depending on the degree of crystallinity and branching the polymer can take different forms. The most common ones are low-density polyethylene (LDPE) and high-density polyethylene (HDPE), the former being investigated in this experiment. Polyethylene is a semi-crystalline thermoplastic and has the chemical formula $(C_2H_4)_n$ [1]. It is formed by the monomer ethene, an illustration of which can be seen in **Figure 5**. With $T_{g\,(LDPE/HDPE)}$ = - 110 °C [1], $T_{m\,(LDPE)}$ = 116 °C and $T_{m\,(HDPE)}$ = 125 °C to 140 °C [26], polyethylene has the lowest glass transition and melting temperatures of all three investigated plastic types. In the presence of oxygen, the polymer starts to decompose significantly at around 250 °C [24]. Plastic bags and packaging films are commonly made from LDPE, while HDPE is used in shampoo bottles, houseware, pipes, or garden furniture [2]. For this experiment, an LDPE packaging foil from an online clothing store was used.

2.1.5 Polypropylene (PP)

Chemical formula	$(C_3H_6)_n$
Monomer name	Propene (aka propylene)
Glass transition temperature	- 20 °C to - 10 °C
Melting temperature	157 °C (isotactic)
Degradation temperature	250 °C
Share of global plastic waste	19 %
Common applications	Food packaging, sweet wrappers, microwave containers, etc.

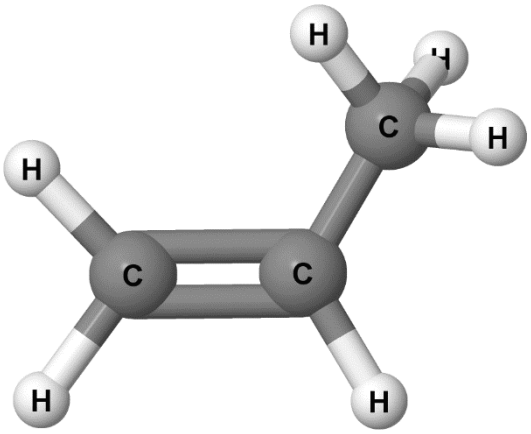

Figure 6: Propene monomer. Illustration created with Jmol [52].

With 19 %, polypropylene (PP) is in second place for both European plastic production [2] and global plastic waste [25]. As described in chapter 2.1.1 "Chemical Structure of Plastics", the polymer chains of PP can be isotactic, syndiotactic, or atactic. Commercially available PP typically consists of three-quarters isotactic and one-quarter atactic polymer chains, resulting in a semi-crystalline structure. PP has the chemical formula $(C_3H_6)_n$ [1]. **Figure 6** shows an illustration of PP's monomer propene. Its glass transition temperature T_g lies between – 20 °C and – 10 °C [1] and its melting point at 157 °C in the case of isotactic PP [26]. Like PE, PP has a thermal-oxidative degradation temperature of 250 °C [24]. Polypropylene is most commonly used as food packaging, sweet wrappers, bottle caps, microwave containers, pipes, and in automotive parts [2]. For this experiment, a candy box made from PP was used.

2.1.6 Polyethylene Terephthalate (PET)

Chemical formula	$(C_{10}H_8O_4)_n$
Monomer name(s)	Ethane-1,2-diol (aka ethylene glycol) and terephthalic acid
Glass transition temperature	73 °C to 78 °C
Melting temperature	250 °C to 255 °C
Degradation temperature	350 °C
Share of global plastic waste	11 %
Common applications	Water bottles, detergent containers, textiles, etc. [2]

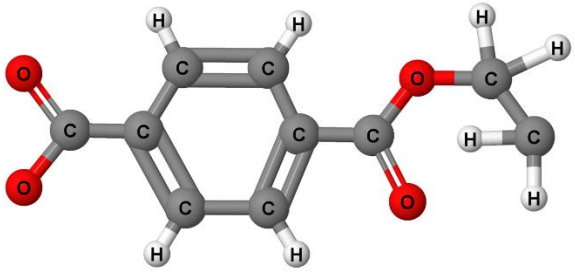

Figure 7: Terephthalic acid and ethane-1,2-diol comonomer. Illustration created with Jmol [52].

Polyethylene terephthalate, commonly known as PET, contributes 11 % of global plastic waste [25]. It comes third in global plastic waste, although with 8 % of plastics produced in Europe, it comes in fifth place in plastic demand, after PP, PE, PVC, and PUR [2]. PET's chemical formula is $(C_{10}H_8O_4)_n$ and it is a copolymer synthesized from the monomers ethane-1,2-diol and terephthalic acid [1]. **Figure 7** shows an illustration of the two monomers forming a combined comonomer. Its glass transition temperature and melting point are the highest of all three examined plastic types with T_g between 73 °C and 78 °C [1] and T_m between 250 °C and 255 °C [26]. Also, the thermal-oxidative degradation temperature is the highest of all three plastic types with weight loss starting at around 350 °C [24]. PET is most widely known for its use in water and soft drink bottles but has many different applications, for example as detergent containers and in various textiles, including clothing [2]. For this experiment, a PET water bottle was used.

2.2 Environmental Plastic Pollution

The vast number of plastic items being produced each year is proof of how important the material is to us and our everyday lifestyle. Most of them, however, are not meant to be used for long periods of time. This is especially true for packaging material, the largest end-use market of plastic converters [2] with an intended use phase of less than 6 months [25]. After the end of its intended use phase, plastic is discarded, recycled, landfilled, or incinerated. Inevitably, some of it ends up in the environment where it breaks down into smaller and smaller pieces, ultimately fueling the so-called "microplastic cycle". While the problem of environmental plastic pollution is mostly a problem of mismanaged or non-managed plastic waste, some findings suggest that even plastics that are properly treated in a waste incineration plant or well-managed landfills could contribute to the microplastic cycle. The following paragraphs examine possible plastic pathways into the environment as well as the microplastic cycle itself. After that, the oftentimes ambiguous definitions of the terms macro-, micro- and nanoplastics are discussed. Although often overlooked, nanoplastics are thought to pose the greatest threat of the three, due to their high number concentrations and small particle sizes. The chapter ends with possible impacts of plastic pollution on environmental and human health.

2.2.1 Pathways into the Environment

With 39.9 %, packaging material accounts for the bulk of the 61.8 megatons of plastics produced in Europe in 2018. With a recycling rate of 42 %, more than half of the collected plastic packaging waste in Europe goes to landfills or energy recovery facilities [2]. Although this does not include packaging waste that could not be collected and therefore might end up in the environment untreated, most of the plastic waste in Europe is retrieved and managed properly. This is not the case for all parts of the world. Especially in many parts of Asia and Africa, the bulk of plastic waste is mismanaged [25]. Landfilled or improperly discarded plastic can be carried away by wind or by water during flooding and often ends up in rivers, where it is deposited in sediments or ultimately reaches the sea. It is estimated that 15 % to 40 % of global plastic waste ends up in the ocean. By 2050, the amount of plastic waste being released to the ocean is estimated to reach 32 megatons per year. Once in the environment, plastic debris degrades into smaller and smaller pieces, ultimately forming secondary micro- and nanoplastics. This happens mostly by photo-oxidative or mechanical degradation [1].

Micro- and nanoplastics can also reach the environment on more direct pathways. Directly released particles are called primary micro- and nanoplastics. Examples for primary micro- and nanoplastics are microbeads in cosmetic and cleaning products or plastic fibers produced during the washing of clothing [16]. Although most of the plastic particles are removed during wastewater treatment, a large amount of microplastics is still released to the environment by wastewater treatment plants. Depending on whether the treatment plants employ two or three treatment phases, 88 % to 97 % of microplastics are removed [27] with one study finding similar values for the removal of nanoplastics below 400 nm [28]. Still, due to the high influent particle concentrations, Sun et al. (2019) find a median value of $2 * 10^6$ microplastic particles per day and wastewater treatment plant, that are discharged directly into the environment [27]. Also supposedly well-managed plastic waste can ultimately lead to environmental plastic pollution with microplastics being found in landfill leachate [29] and in incineration plant bottom ash, which in turn is either landfilled itself or used as constructing material or in agriculture [30]. From there, micro- and nanoplastics can leach into the environment or be picked up by the wind, making wastewater treatment plants, landfills and waste incineration plants possible sources of plastic pollution of water, soil, and air.

2.2.2 The Microplastic Cycle

For a long time, it was assumed that all plastic in the environment would eventually end up in the ocean, either floating at the surface, sinking to the seafloor, being suspended in the water column, or being washed up at beaches [1]. Only recently have researchers begun to think of plastic as being cycled in the environment, a concept that is already used for many other environmentally relevant substances. The so-called “Microplastic Cycle” aims to give a better understanding of where plastic particles aggregate and on which pathways they are transported. A sketch of the microplastic cycle can be seen in **Figure 8**. The arrows show fluxes between the pools of aggregated microplastics. With the hydrosphere, atmosphere, geosphere, and biosphere as microplastic pools, plastic particles are cycled through all four major parts of the earth system [31].

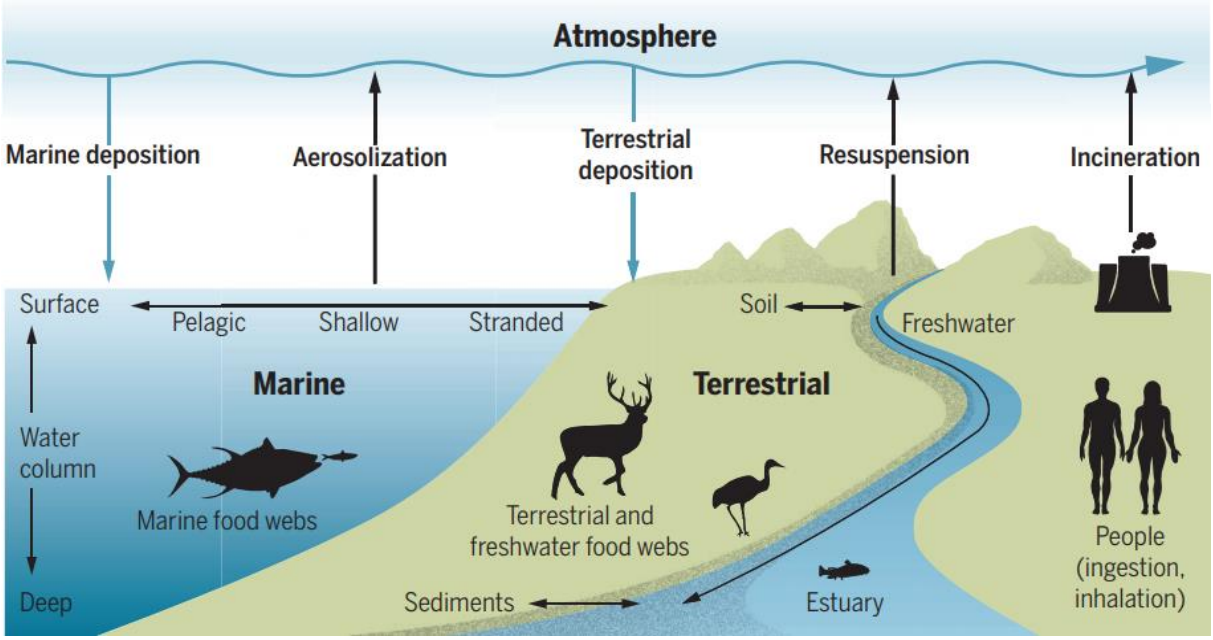

Figure 8: Proposed microplastic cycle. Illustration by Rochman and Hoellein, 2020 [31].

The fluxes between terrestrial and marine environments and the atmosphere displayed in **Figure 8** include wet and dry deposition of plastic particles over land and the ocean as well as their ways back into the atmosphere through aerosolization of sea spray, resuspension from the ground, and by ejection from incineration plants. Plastic particles get picked up by the wind and are transported in the atmosphere, reaching even the remotest places of our planet. Microplastics have been found in Arctic snow [5] and secluded mountain areas in the French Pyrenees [7] and the Swiss Alps [5]. Unsurprisingly, the amount of microplastic fallout increases for highly populated areas with atmospheric microplastic deposition being observed in cities like Paris, France [4], Bremen, Germany [5], and Dongguan, China [6]. It is easy to imagine, that plastic particles similarly reach the ocean. A reverse mechanism that brings plastic particles from the ocean back into the atmosphere was recently suggested by Allen et al. (2020). Microplastics are likely to be picked up by the atmosphere from the sea surface through bubble burst ejection, alongside with sea salt, bacteria, viruses, and algae [32].

2.2.3 Macro-, Micro- and Nanoplastics

One major factor in determining the risk posed by plastics in the environment is the particle size. Therefore, clear definitions of the investigated particle sizes are necessary. For this experiment, plastics are categorized according to their size into macroplastics, microplastics, and nanoplastics. **Table 1** shows these three classifications and their

corresponding size ranges, as defined for this thesis. It should be noted, that not the full nanoplastic size range was examined during the experiment. The measured aerosol particles were all below 50 nm in accordance with the nano-DMPS setup shown in chapter 3.2 “Experimental Setup”.

Table 1: Size classifications of macro-, micro-, and nanoplastic as defined in this thesis.

Classification	**Size (in the largest dimension)**
Macroplastic	≥ 5 mm
Microplastic	1 µm – 5 mm
Nanoplastic	< 1 µm

As stated in chapter 1.1.2 “Health Risk of Airborne Plastic Particles”, there is no widely accepted definition of nanoplastic. Four of the five papers on atmospheric plastic pollution mentioned in the introduction section of this thesis do not differentiate between micro- and nanoplastics. Two of them (Dris et al., 2016 and Gasperi et al., 2018) do not measure in the nano-range at all, setting their lower detection limit to 50 µm. Fibers below this threshold were not measured or taken into account. Only Allen et al. (2019) give a clear indication of the size boundary between micro- and nanoplastics with nanoplastics being defined as being below 1 µm in the largest dimension. Another definition of nanoplastics sets the upper size limit at 100 nm. This value is derived from the current definition of manufactured nanomaterials [33]. Gigault et al. (2018) discuss this problem in their paper “Current opinion: What is a nanoplastic?” alongside a second definition discrepancy. While some authors distinguish between primary and secondary micro- and nanoplastics as described in chapter 1.1.3 “Origin of Airborne Nanoplastics”, others only label unintentionally produced plastic particles below a certain size threshold as nanoplastics. According to this definition, there are no primary nanoplastics with intentionally produced plastic particles being called “manufactured nanomaterials” [33]. The most common definition distinguishes between intentionally produced primary and unintentionally produced secondary micro- and nanoplastics. To add to the confusion, there are a few more plastic particle definitions to be found in literature, such as mesoplastic, plasticle or mini-microplastic [1]. All of this shows clearly that consistent plastic particle size definitions and classifications still need to be developed and accepted in scientific research.

2.2.4 Impacts on Environmental and Human Health

Once in the environment, it is only a matter of time until plastic particles are ingested by animals and thus enter the food chain. This can cause blockages of the airways or the digestive tract, internal injuries, and reduced energy consumption, ultimately leading to starvation. Another concern is toxicological effects. Although the polymers themselves are considered to be biochemically inert, additives and adsorbed pollutants, such as heavy metals, may leach from the plastics. Possible consequences include disturbed hormone levels, development defects, delayed maturity, and reproductive disorders. As these contaminants are passed through the food chain, they can bioaccumulate, leading to increased concentrations on each trophic level [34]. This phenomenon has mostly been brought to public attention in the case of shellfish, which is known to be a source of microplastic in the human diet. However, Senathirajah and Palanisami (2019) have found that roughly 90 % of the plastic ingested by humans comes from drinking water, with microplastic being found in both tap water and bottled water samples all around the world. They estimate that an average person consumes around 5 g of plastic each week – the equivalent of a credit card [35]. Ingestion is the main pathway on which plastic enters our bodies, with additional intake through inhalation and dermal exposure, for example from cosmetic products. The severity of adverse health effects caused by this constant exposure to micro- and nanoplastics is still investigated. Possible toxicological effects include oxidative stress, inflammation, and metabolic disorders [36]. In addition to that, small enough particles can enter cellular tissue [13] and have been shown in simulations to even penetrate cell membranes, ultimately leading to cell death [12]. Polystyrene nanoparticles were found to accumulate in various organs of developing zebrafish, including the brain, indicating they can overcome the blood-brain-barrier. However, little is known about the environmental concentrations of such nanoparticles and thus the actual environmental risk cannot be clearly stated [13]. For the case of airborne microplastics, several studies have shown an increased risk of respiratory diseases in people working in the synthetic textile or flocking industry as well as in VC and PVC manufacturing. Due to their chronically high exposure to airborne microplastics, several occupational diseases have been observed in these workers, such as impaired lung function, lesions of the lower airways, chronic bronchitis and pneumonia, acute respiratory failure, increased risk of lung cancer, etc. [15]. Thus, airborne plastic particles factor into the seven million annual deaths by air pollution, as estimated by the WHO [37].

2.3 Relevant Concepts of Aerosol Physics

To understand the methodology of this thesis, it is necessary to introduce a few key concepts of aerosol physics. The nanoparticle aerosols generated in this experiment are formed by homogeneous nucleation and subsequent condensation of plastic vapor, which is produced by heating and evaporating everyday plastic items. The following paragraphs will therefore deal with homogeneous nucleation and the principles necessary to describe it – the saturation ratio, the Kelvin equation, and a bit of classical nucleation theory.

2.3.1 The Saturation Ratio

The formation of aerosol particles by homogeneous nucleation and subsequent growth by condensation requires a supersaturated vapor. A vapor is supersaturated when its partial pressure p_v is greater than its saturated vapor pressure $p_s(T)$. The ratio of these two pressures is called the saturation ratio S and is given by:

$$S = \frac{p_v}{p_s(T)} . \tag{1}$$

In a volume filled with a mixture of gases (or vapors), the partial pressure p_v is the pressure that gas would have if it were the only gas present in the volume. The total pressure of the mixture equals the sum of the partial pressures of its components, as stated by Dalton's Law. The saturation vapor pressure $p_s(T)$ is the pressure at which the vapor is in mass equilibrium with its liquid (or solid) phase at a certain temperature T. For $p_v = p_s(T)$, evaporation and condensation at the surface of the condensed phase cancel each other out and there is no net mass transfer. In this case, $S = 1$. Is $S < 1$, the vapor is undersaturated and there is more evaporation than condensation at the surface of the condensed phase. For $S > 1$, the vapor is supersaturated, with more condensation than evaporation [38]. **Table 2** summarizes these three saturation conditions.

In this experiment, supersaturation is induced by cooling the generated plastic vapor after the tube furnace. As the vapor cools, the saturation vapor pressure $p_s(T)$ drops faster than the partial pressure p_v and the saturation ratio exceeds 1. This allows for homogeneous nucleation as described in the following paragraph.

Table 2: Characteristics and consequences of undersaturation, saturation, and supersaturation.

Relationship of p_v to $p_s(T)$	Saturation Ratio S	Consequence
$p_v < p_s(T)$	< 1	**Undersaturation** More evaporation than condensation
$p_v = p_s(T)$	= 1	**Saturation** No net mass transfer between vapor and condensed phase
$p_v > p_s(T)$	> 1	**Supersaturation** More condensation than evaporation

2.3.2 Homogeneous Nucleation and the Kelvin Equation

In this experiment, aerosol particles are formed by homogeneous nucleation from supersaturated plastic vapor. This means that there are no condensation nuclei present onto which vapor condensates, as it would be the case for heterogeneous nucleation. Instead, prospective aerosol particles start out as molecule clusters which form as a result of weak attractive, intermolecular forces, such as van der Waals forces. High levels of supersaturation aid this formation of clusters. These clusters are not stable and usually disintegrate soon after their formation. However, if a cluster reaches the critical radius r* – through statistical fluctuation or by merging with other clusters – it becomes a stable droplet and starts to grow by condensation. This critical radius r* depends on the level of saturation and is described by the (rearranged) Kelvin equation:

$$r^* = \frac{2\,\sigma}{n_l\,k\,T\,ln(S)}\ , \tag{2}$$

where σ is the surface tension of the droplet, n_l is the number of molecules per volume, k is the Boltzmann constant, T is the temperature and S is the saturation ratio. For any given S, a particle with r* is in equilibrium and therefore stable. Is it smaller than r*, it evaporates, is it larger, it grows by condensation [38].

2.3.3 Description in Classical Nucleation Theory

The processes involved in the formation of aerosol particles by nucleation are described by classical nucleation theory (CNT). CNT helps to understand what exactly the critical radius is and why a cluster must reach it to become a stable droplet and grow by condensation. The energy that is needed to form a cluster can be described using the Gibbs free energy. Energy is needed to form a surface boundary between the vapor and the liquid phase (described by the surface term $\Delta G_{Surface} = 4\,\pi\,\sigma\,r^2$), while energy is released from the change in the chemical potential μ from vapor (v) to liquid (l) molecules for $\mu_v > \mu_l$ (described by the volume term $\Delta G_{Volume} = -\frac{4\,\pi}{3} n_l\,r^3\,k\,T\,ln(S)$). Together, the surface term and the volume term add up to the nucleation work $\Delta G_{Nucleation}$:

$$\Delta G_{Nucleation} = 4\,\pi\,\sigma\,r^2 - \frac{4\,\pi}{3} n_l\,r^3\,k\,T\,ln(S)\,. \qquad (3)$$

As in the Kelvin equation (2) above, σ is the surface tension of the droplet, n_l is the number of molecules per volume, k is the Boltzmann constant, T is the temperature and S is the saturation ratio. In the equilibrium state $\frac{\partial(\Delta G_{Nucleation})}{\partial r} = 0$ equation (3) can be solved for r, resulting in the Kelvin equation (2). **Figure 9** shows $\Delta G_{Surface}$, ΔG_{Volume}, and the resulting nucleation work $\Delta G_{Nucleation}$ plotted against the cluster radius r. If there is supersaturation (S > 1), $\Delta G_{Nucleation}$ reaches its extremum at the critical cluster radius r* and a stable droplet is formed. If S ≤ 1, the volume term is positive and $\Delta G_{Nucleation}$ grows without bound. In this case, there is no stable cluster radius r*.

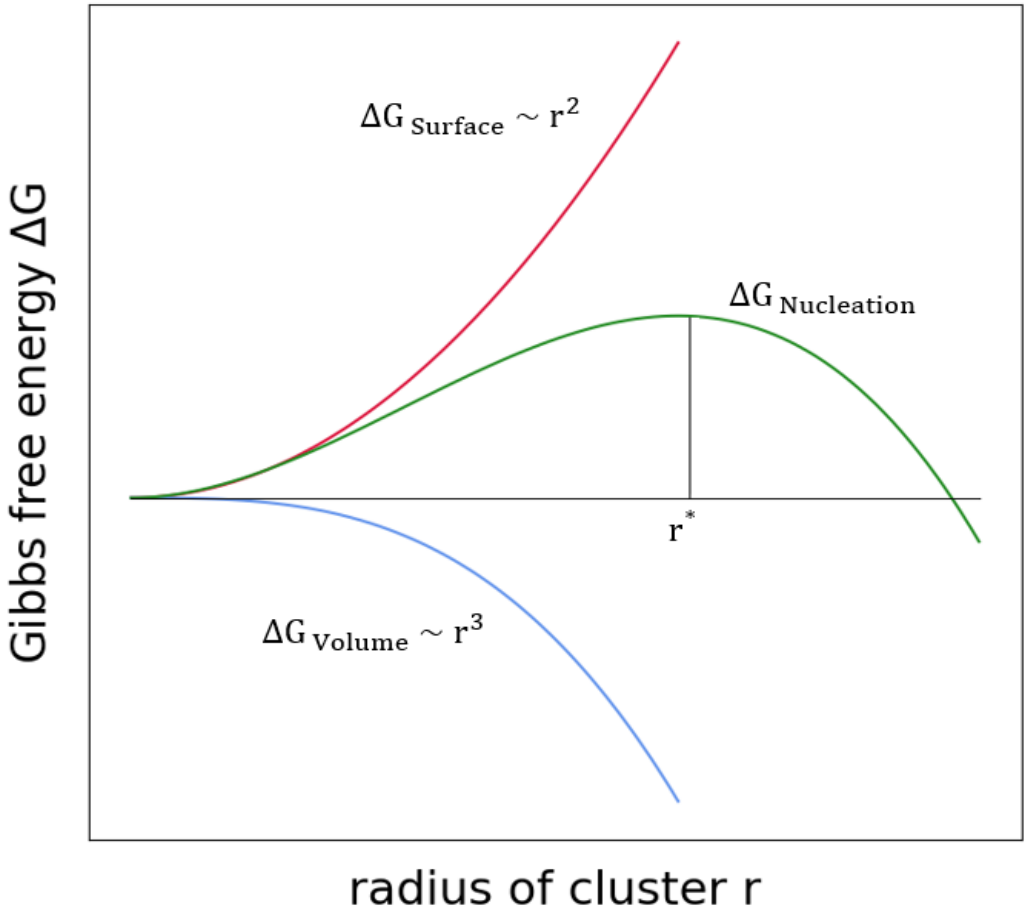

Figure 9: Surface term (red), volume term (blue) and $\Delta G_{Nucleation}$ (green) plotted versus the cluster radius r for the case S > 1.

3 Methodology and Experimental Setup

The goal of this experiment was to generate nanoplastic aerosols by heating plastic in a tube furnace and cooling the formed vapor to induce homogeneous nucleation and condensation of nanoparticles. Number size distributions of the aerosols for different temperatures and plastic types (PE, PP, and PET) were recorded with a Differential Mobility Particle Sizer (DMPS) system. This experimental setup is based on Scheibel and Porstendörfer (1983). The obtained data on electrical mobility diameters and particle number concentrations was evaluated using a python program coded specifically for this purpose. The different number size distributions were plotted and their defining characteristics, like maximum particle concentrations, mode particle diameters, and distribution widths, were discussed and compared. The following paragraphs describe the preparation method for the PE, PP, and PET macroplastics used as aerosol material for evaporation in the tube furnace as well as the experimental setup and the software used for data collection. The chapter ends with a brief discussion of uncertainty sources within the experiment.

3.1 Preparation of PE, PP, and PET Samples

The samples used for aerosol generation in this experiment were everyday plastic items: a low-density polyethylene (LDPE) packaging foil from an online clothing store, a polypropylene (PP) candy box, and a polyethylene terephthalate (PET) water bottle. To minimize the effect of additives (in this case especially coloring agents), only colorless plastic was used. All samples were mostly transparent before heating, suggesting a low degree of crystallinity. Only the LDPE foil showed a slight white translucency. The different plastic materials were washed with water and cut into flakes of approximately 1 cm length and 0.5 cm width. A photograph of the washed and cut up LDPE, PP, and PET flakes can be seen in **Figure 10** below.

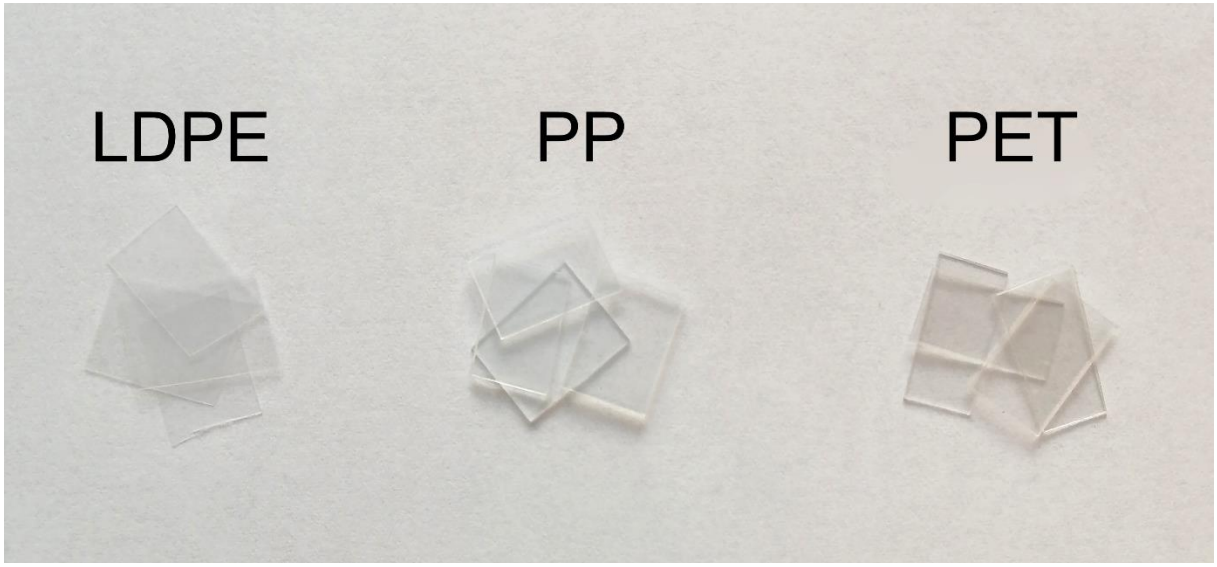

Figure 10: LDPE, PP, and PET flakes after preparation for the experiment.

For heating in the tube furnace, the flakes were placed into handmade aluminum foil spoons. In the preparation phase of the experiment, background measurements of empty aluminum foil spoons at temperatures up to 300 °C were made to check that they would not distort the measured particle concentrations. The spoons showed no additional background. To ensure that all samples get heated at the same position inside the tube furnace, near the center of the heating area, all spoons were made sure to have a length of 20 cm. For PP and PET, 10 flakes each were used for one sample. For the thinner LDPE foil, 15 flakes were used to obtain a similar end volume of plastic before heating. **Figure 11** shows the prepared samples, ready to be inserted into the tube furnace.

Figure 11: LDPE, PP, and PET flakes inside aluminum spoons, ready for heating in the tube furnace.

3.2 Experimental Setup

The experimental setup for this experiment consisted of three main components – a tube furnace, a nano Differential Mobility Analyzer (nano-DMA), and a Faraday Cup Electrometer (FCE). The nano-DMA and the FCE together form a so-called Differential Mobility Particle Sizer (DMPS), that applies different voltages in a defined voltage range, classifies aerosol particles based on their electrical mobility, and counts the classified particles. In the following pages, the used tube furnace, aerosol charger, DMA, and FCE will be briefly described.

3.2.1 Tube Furnace

After preparation, the aluminum foil spoons with the plastic flakes were inserted into a quartz glass tube inside a tube furnace. The glass tube was connected to a stream of compressed and dried air with a flow rate of 1.4 liters per minute (lpm). This air flow carries evaporated material from the plastic sample with it, as described by Scheibel and Porstendörfer (1983) [18]. **Figure 12** illustrates this furnace setup with a quartz glass tube and a spoon filled with plastic flakes. After the furnace, the plastic vapor was diluted with another 1.4 lpm of compressed air and then passed through a water-cooling tube set to 15 °C. The cooling of the vapor induces homogeneous nucleation of aerosol particles as described in chapter 2.3 “Relevant Concepts of Aerosol Physics”. The furnace used in this experiment was a Carbolite Gero Tube Furnace EHA Model with a heated length of 300 mm and a maximum temperature of 1200 °C. The quartz glass tube had a length of 38 cm and a diameter of approximately 1.5 cm. The aluminum foil spoons had a length of 20 cm.

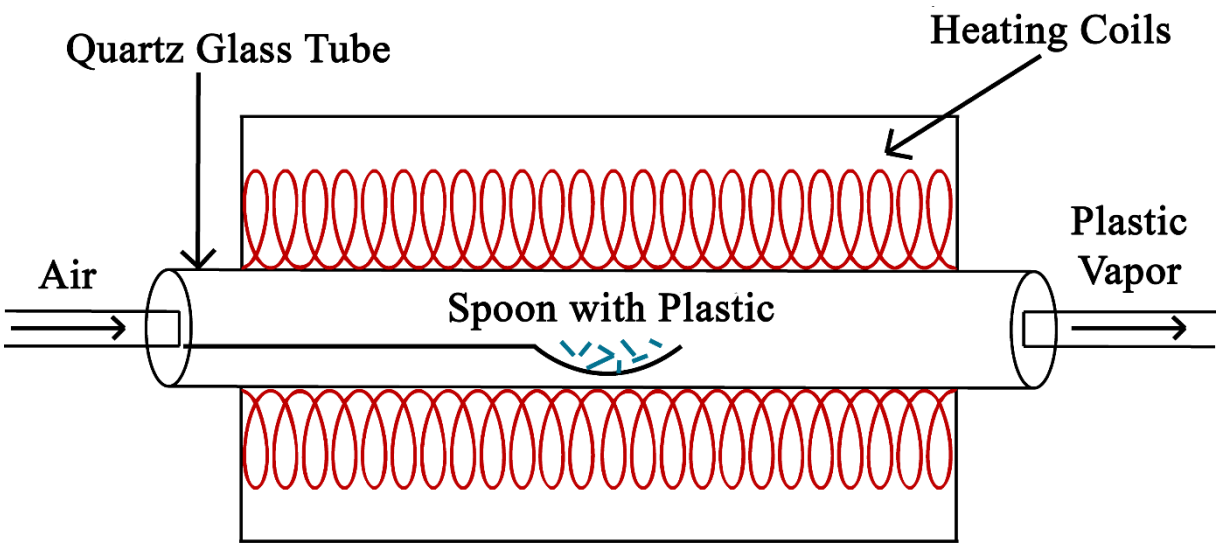

Figure 12: Illustration of the tube furnace with a quartz glass tube and a plastic filled spoon.

3.2.2 Aerosol Charger

An aerosol charger (also called aerosol neutralizer) is used to apply charges to the aerosol particles before they enter the DMA. After passing through the aerosol charger, the aerosol is in a stationary charge distribution. This charge distribution can be modeled using the numerically solvable Fuchs limiting sphere charge distribution model or the analytically solvable Wiedensohler approximation [39]. In this experiment, an Americium (^{241}Am) aerosol charger was used. This radioactive source charger creates a bipolar ion atmosphere in which positive and negative ions are present. Through the process of diffusion charging, charges are attached to the aerosol particles and the aerosol is charged [40]. **Figure 13** shows the charging probabilities of negatively charged aerosol particles in a bipolar ionic atmosphere with charging states between one and five elementary charges, as predicted by Fuchs' limiting sphere charge distribution model. As the illustration shows, the smaller the particles, the less likely they are to carry multiple charges. The same is true for positively charged particles, although here the charging probabilities are slightly lower in comparison to negatively charged particles [41]. The probability of finding particles with double charge is 0.01 at a particle diameter of 50 nm and approaches zero at about 30 nm. As the upper size limit of this experiment was at 47.8 nm and most of the measured particles had a mobility diameter below 20 nm, only singly charged particles were expected and therefore no data inversion was applied.

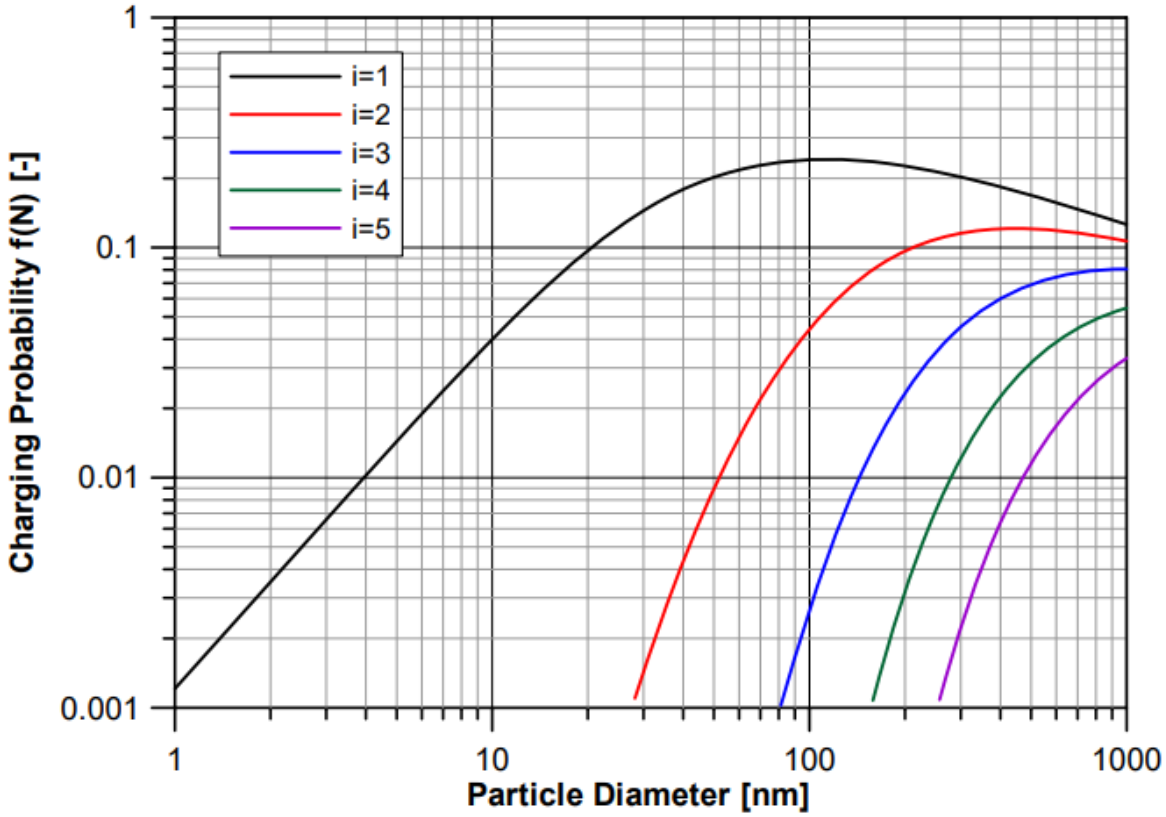

Figure 13: Charging probabilities as predicted by Fuchs' limiting sphere model for negatively charged aerosol particles in a bipolar ionic atmosphere with charging states i from one to five. Illustration by Steiner, 2011 [41].

3.2.3 Differential Mobility Analyzer (DMA)

Differential Mobility Analyzers (DMAs) are commonly used instruments to classify aerosol particles based on their electrical mobility. A DMA consists of an inner and an outer electrode. A high voltage is applied to the inner electrode, while the outer one is grounded, creating an electric field. At the top of the DMA, the charged aerosol flow Q_A and the sheath air flow Q_{Sh} flow into and through the DMA. Aerosol particles with a charge opposite to the polarity of the inner electrode are drawn towards the center and particles with the right electrical mobility Z for the applied voltage V reach the outlet slit of the DMA. From there, the monodisperse aerosol Q_S is led to the FCE for measurement, while the sheath air and the rest of the particles exit the DMA as excess air Q_{Ex} [42]. By varying the applied voltage, monodisperse aerosols with particles of different electrical mobilities can be classified.

Figure 14 shows this basic working principle of a DMA. The original figure from Intra and Tippayawong (2008) was minorly adapted to better visualize the labels for the aerosol inlet flow Q_A, the sheath air flow Q_{Sh}, the excess air flow $Q_{Ex,}$ and the monodisperse aerosol sample outlet flow Q_S.

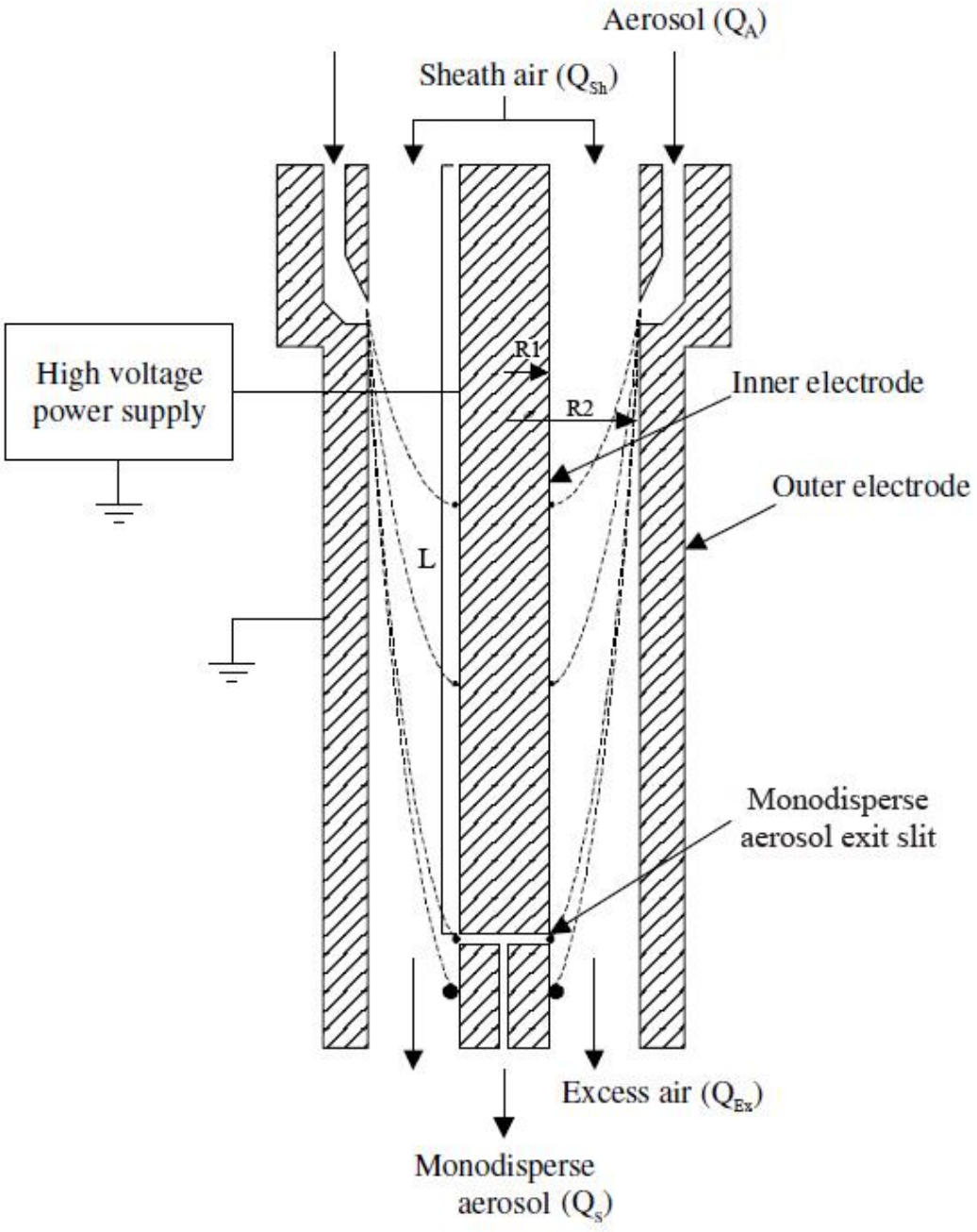

Figure 14: Basic working principle of a differential mobility analyzer (DMA). Adapted from Intra and Tippayawong, 2008 [42].

This method of aerosol particle classification is based on equation (4), which shows, that the electrical mobility Z of a particle is inversely proportional to the particle's electrical mobility equivalent diameter D_p (in this thesis commonly shortened to electrical mobility diameter or particle diameter). For Reynolds numbers Re < 1, corresponding to laminar flow conditions within the DMA, Z is given by:

$$Z = \frac{neC_S(D_p)}{3\pi\eta_{air}D_p} \tag{4}$$

Here, n is a whole number giving the number of charges on the particle, e is the elementary charge, C_s is the Cunningham slip correction factor for particles with diameters D_p near the mean free path of air molecules, and η_{air} is the dynamic viscosity of air. Another way of expressing the electrical mobility Z is through the geometrical and operational parameters of the DMA. In this case, Z is given by:

$$Z = \frac{\ln\left({}^{R_2}/_{R_1}\right)}{V\ 2\pi\ L}\ \frac{(Q_{Sh} + Q_{Ex})}{2} \tag{5}$$

where R_2 is the radius of the outer DMA electrode, R_1 the radius of the inner DMA electrode, V is the applied voltage, L is the DMA channel length, Q_{Sh} is the sheath air flow rate and Q_{Ex} is the excess air flow rate. By equating (4) and (5), the electrical mobility equivalent diameter can be calculated [41]. In this experiment, this was done by the program EMS, which is presented in chapter 3.3 "Data Collection and Evaluation".

The DMA used during this experiment was a University of Vienna type DMA. Winklmayr et al. developed this kind of DMA design in 1990 to maximize flow stability at high flow rates, which helps to minimize diffusional losses of aerosol particles [42]. A variation of this original Vienna-type DMA is the Vienna-type nano-DMA with a shorter channel length and smaller aspect ratio of the channel length L to the radii of the two electrodes R_2 and R_1. The nano-DMA is particularly well suited to measure particles below 10 nm [43]. The Vienna-type nano-DMA used during this experiment has a channel length of L = 15 mm, an inner electrode radius of R_1 = 17.5 mm, and an outer electrode radius of R_2 = 24.1 mm. The flow rates were set to a nominal value of Q_A = 2.8 lpm for the aerosol flow and Q_{Sh} = 18.5 lpm for the sheath flow. The voltages applied to the electrodes ranged from 1 V to 10.000 V to measure in a particle size range from 0.7 nm to 47.8 nm. However, at the lower end of this range, the voltage is often not correctly set by the EMS software and therefore particles below a size of 2 nm were not considered. This is also in accordance with the FCE measurement range.

3.2.4 DMA Resolution and Transfer Function

As described by Flagan (1999), the resolution of a DMA is defined as the ratio between the particle mobility at the peak of the DMA's transfer function to its full-width-half-maximum (FWHM). The transfer function Ω(Z, Z*) is the probability, that a particle with mobility Z makes it to the outlet slit of the DMA and is included in the DMA's particle classification when the DMA is set up to classify particles with mobility Z*. More precisely, Ω(Z, Z*) is the so-called column transfer function, as described by Knutson and Whitby in 1975 [44]. The column transfer function does not include the detector sensitivity or particle losses outside of the classification region of the DMA. To include these possible sources of uncertainty, a detector response function S(Z) and the penetration efficiency $\eta_{pen}(Z)$ are introduced. Together with the column transfer function Ω(Z, Z*), this leads to the system transfer function $T_{sys}(Z, Z^*)$:

$$T_{sys}(Z, Z^*) = S(Z) * \eta_{pen}(Z) * \Omega(Z, Z^*) \quad (6)$$

The DMA transfer function is broadened and therefore the resolution is reduced, when particles deviate from their ideal pathways through the DMA due to Brownian diffusion [45]. The smaller the particles, the more they diffuse, as is evident from the Brownian diffusion coefficient D:

$$D = \frac{kTC_S}{3\pi\eta_{air}D_p} \quad (7)$$

In this so-called Stokes-Einstein equation (7), k is the Boltzmann constant, T is the absolute temperature, C_s is the Cunningham slip correction factor for particles with diameters near the mean free path of air molecules, η_{air} is the dynamic viscosity of air and D_p is the particle diameter [38].

As the transfer function is not known for the given experimental setup, a different measure of resolution needs to be applied. Flagan (1999) showed that the limiting resolution of a DMA for non-diffusive particles under the condition of balanced flows ($Q_A = Q_S$) is given by the flow rate ratio β:

$$\beta = \frac{Q_A + Q_S}{Q_{Sh} + Q_{Ex}} \quad (8)$$

For this experiment, a flow rate ratio and thus a limiting resolution of β = 0.15 was aimed at. To achieve this resolution, an aerosol flow rate of $Q_A = Q_S = 2.8$ lpm and a sheath flow rate of $Q_{Sh} = Q_{Ex} = 18.5$ lpm was used.

3.2.5 Faraday Cup Electrometer (FCE)

To measure the particle concentration of the charged, monodisperse aerosol exiting the DMA, a Faraday Cup Electrometer (FCE) was used. The FCE was operated with an aerosol inlet flow rate of Q_{FCE} = 1.5 lpm. As described in the user's manual of the TSI 3068B FCE used during this experiment, the charged aerosol particles flowing into the FCE are deposited on a high-efficiency conductive filter inside a Faraday cup. The current from this cup is measured with an electrometer current sensor. With knowledge of the aerosol charge distribution (see chapter 3.2.2 "Aerosol Charger"), the particle concentration N can be calculated with the following equation:

$$N = \frac{I}{n\, e\, Q_{FCE}} \tag{9}$$

where N is the aerosol particle concentration, I is the electrometer current, n is the number of charges per particle, e is the elementary charge and Q_{FCE} is the volumetric aerosol flow rate into the FCE in cm^3/s. **Figure 15** shows the basic working principle of an FCE as pictured in the user's manual of the FCE model TSI 3068B. The instrument has an RMS noise current of 1 fA at an averaging time of one second (as was used during the experiment). The current accuracy is ± 2 % of the measured current or ± 5 fA (corresponds to 1250 particles/cm^3 at the used flow rate of 1.5 lpm), whichever is greater. The particle size range that can be measured by the FCE is 2 nm to 5000 nm [46].

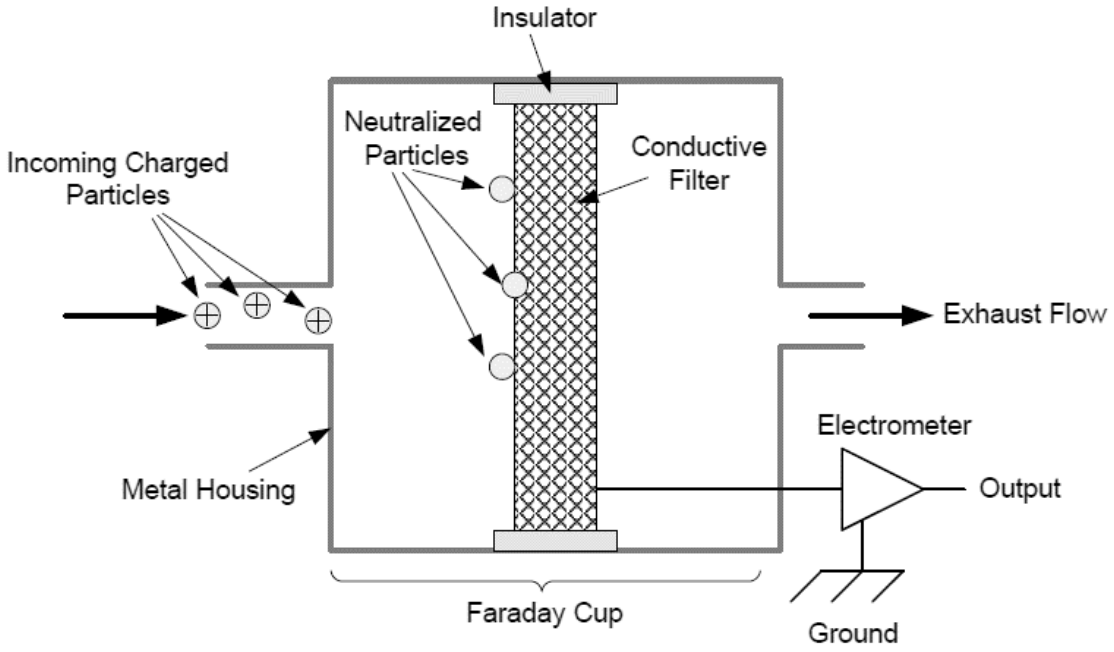

Figure 15: Basic working principle of a Faraday Cup Electrometer. Illustration by TSI Incorporated, 2009 [46].

3.2.6 The Final Setup

Besides the main components described above, there were some smaller parts necessary to conduct this experiment. They consisted mainly of tubing to connect the different devices, two valves to regulate the air flow going through the furnace and through the DMA, a pump for the DMA sheath flow as well as the FCE, the cooling tube to cool the vapor after the furnace, a high voltage (HV) generator, an electrical control panel, and a laptop to run the measurement software on. The sheath flow for the DMA consisted of more tubing, a pump, a dryer with silica gel to stabilize the air flow from the pump and dry the air going through the volume, an 18.5 lpm critical orifice to control the air volume per minute that flows through the DMA and a HEPA (high-efficiency particulate air) filter to filter out aerosol particles that might have reached the sheath flow. Furthermore, there were two exhausts, each with a HEPA filter – one after the pump and one directly before the FCE to release the excess aerosol that was not used by the FCE. An illustration of the final setup can be seen in **Figure 16** below.

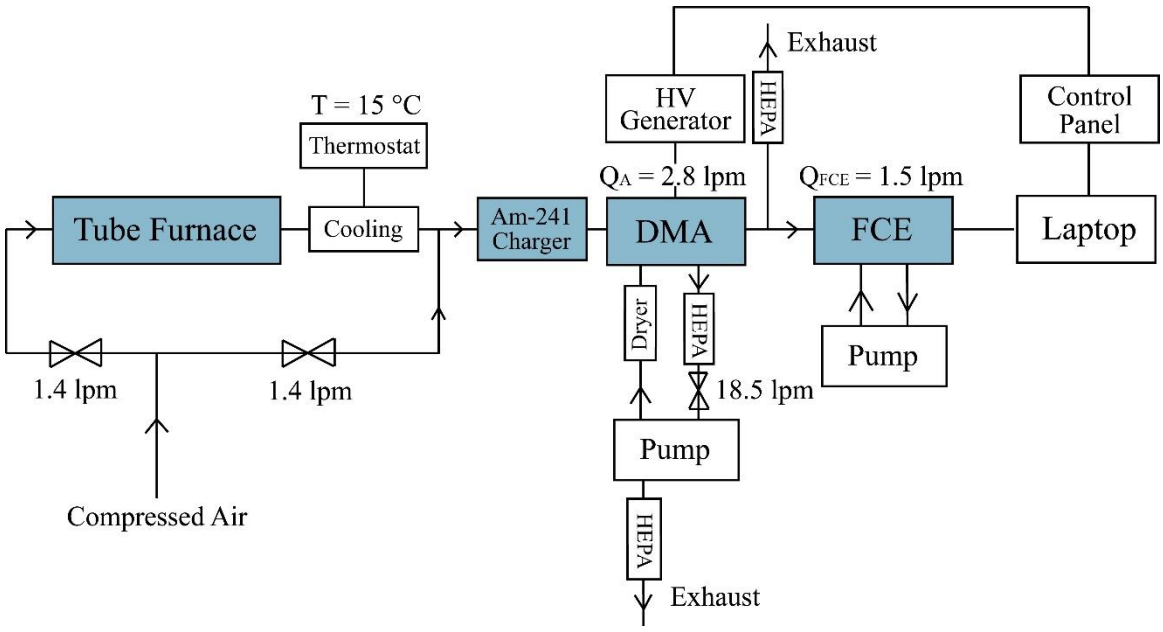

Figure 16: Illustration of the experimental setup. The main components discussed in this chapter are highlighted in blue.

3.3 Data Collection and Evaluation

During the measurement, two software programs were used for data collection. The DMA voltages and corresponding particle mobility diameters were controlled and recorded using the EMS-10 Control Center Operating Software EMSCC 1.4 (EMS) [47]. The FCE signal and calculated particle concentrations were read out with the Aerosol Instrument Manager Software (AIM) [48]. EMS was operated in the "Analyzer" operating mode with high resolution, which sections the 1 V – 10.000 V range from the HV-generator into 97 channels. With AIM, the measured currents from the FCE and the corresponding particle concentrations were recorded. After the measurement, the data from EMS and AIM was exported into two separate CSV files. To match the particle mobility diameters from the EMS file to the particle concentrations from the AIM file, average over the measured EMS runs, and plot the resulting number size distributions, a python 3.7 program was written. To fit the distributions and find the maximum particle concentrations, mode particle diameters, and distribution widths, the program Fityk [49] was used.

Figure 17 shows the particle concentration recorded by AIM as a function of time for a measurement of PP at 220 °C. The peaks correspond to ten runs in EMS. By averaging over these runs and matching the averaged particle concentrations to the corresponding particle diameters recorded by EMS, the aerosol's number size distribution shown in the following chapter was obtained.

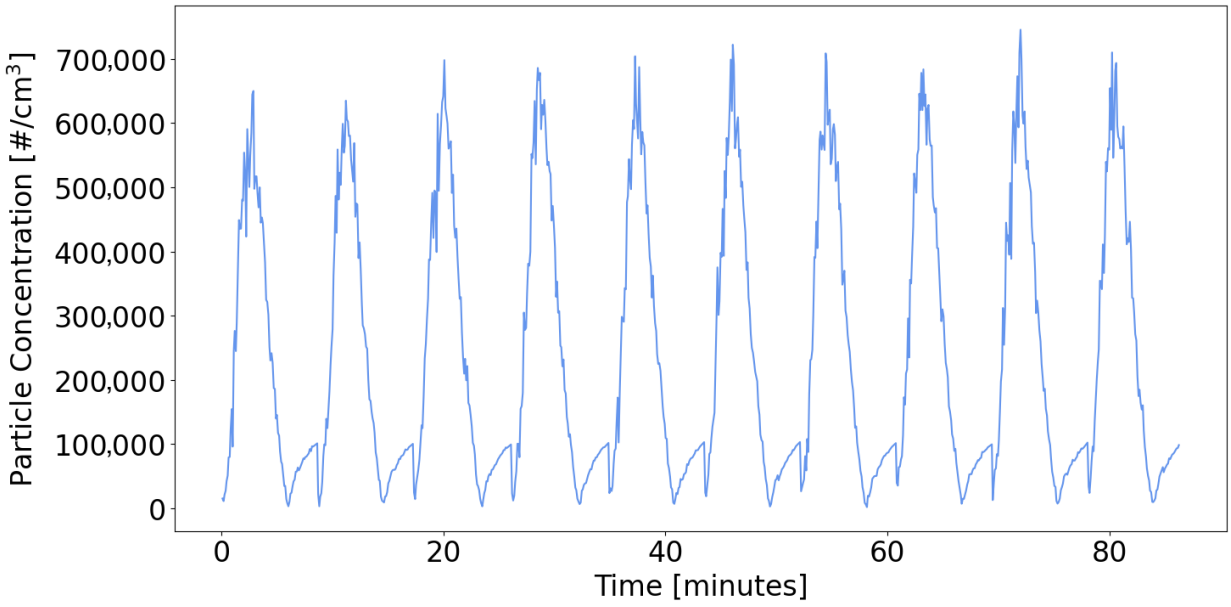

Figure 17: Particle concentration over time recorded with AIM during a measurement of PP at 220 °C.

3.4 Uncertainty Estimation

The following paragraphs concern themselves with the measurement and averaging uncertainties associated with the experiment conducted for this thesis. To obtain the number size distributions shown in the following chapter, 10 EMS runs per temperature and plastic type were recorded and averaged, as described above. **Figure 18** shows the number size distribution of PP at 220 °C as a solid blue line and the standard deviation associated with the averaging of the EMS runs as dashed lines.

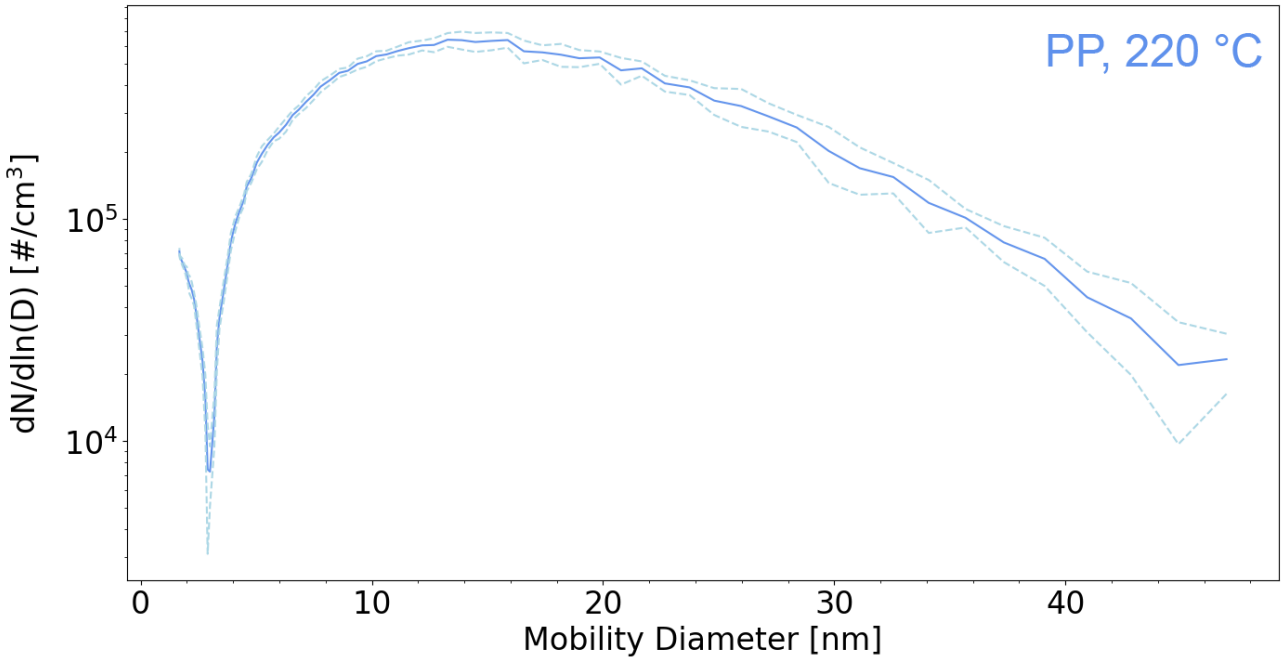

Figure 18: Number size distribution of PP at 220 °C (solid line) and standard deviation of concentrations averaged over 10 EMS runs (dashed lines).

The uncertainties from the measurements themselves for the same number size distribution can be seen in **Figure 19**. The uncertainty values for the particle concentrations are the sum of the FCE uncertainty of 2 % of the measured current (not less than 5 fA) plus $\sqrt{N}$, where N is the particle count, as a measure of the statistical variation of each measurement point. The uncertainty values for the mobility diameters result from the DMA resolution of $\beta = 0.15$. A discussion of the DMA resolution and the equation with which it is calculated can be found in chapter 3.2.4 “DMA Resolution and Transfer Function”. **Figure 18** and **Figure 19** are exemplary for the number size distributions in the “Experiment and Results” chapter, in which uncertainty bars were omitted for reasons of clarity and comprehensibility.

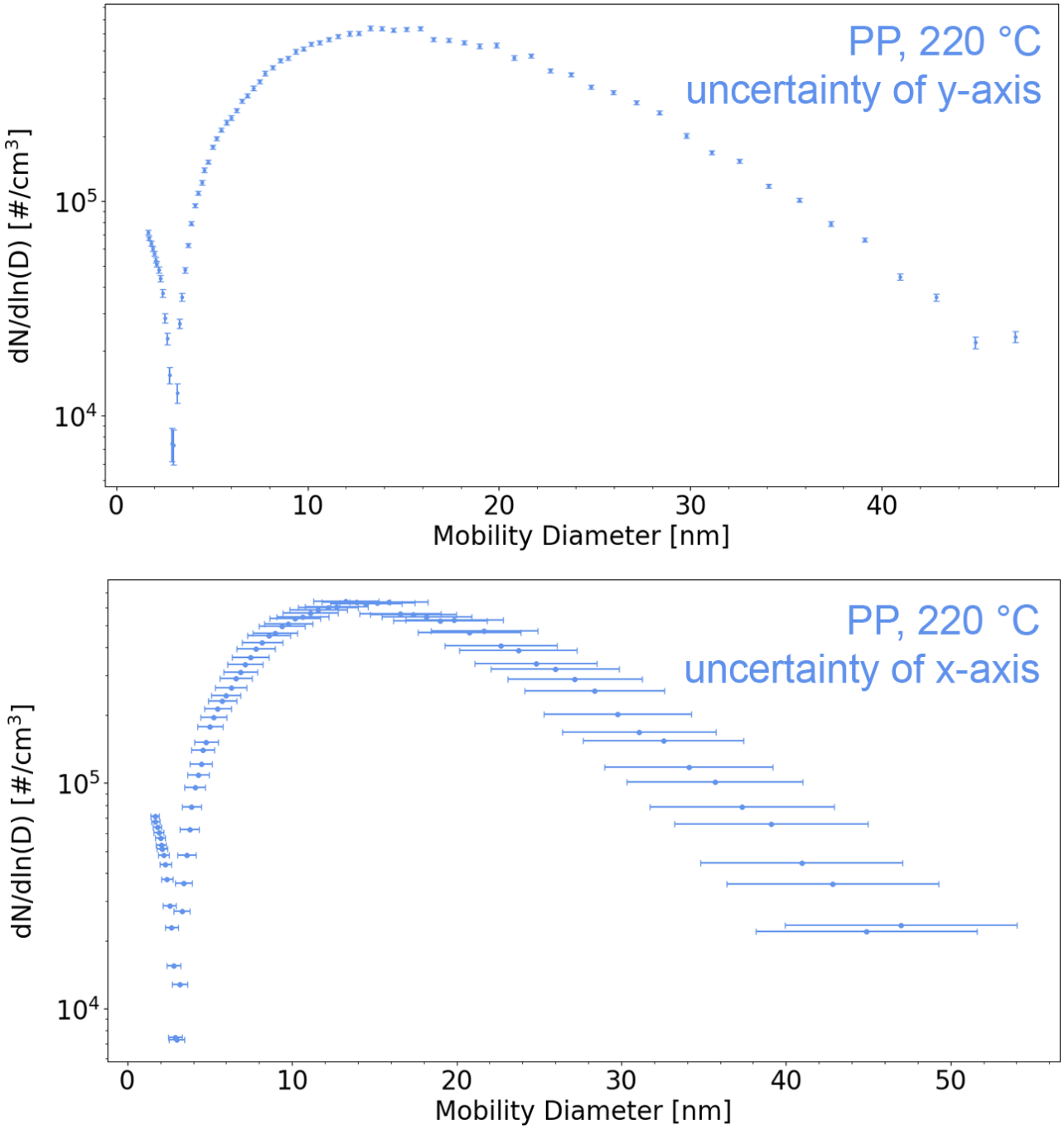

Figure 19: Number size distribution of PP at 220 °C with uncertainty bars for the measured particle concentrations (top) and mobility diameters (bottom).

The measuring instruments used during the experiment and their uncertainties are listed in **Table 3**. Another source of uncertainty is the amount of plastic used per sample. As described in chapter 3.1 “Preparation of PE, PP, and PET Samples” 10 flakes of PP or PET or 15 flakes of LDPE were used per measurement. Should this experiment ever be repeated, it is advised to weigh the plastic instead of cutting it into roughly same-sized pieces. This would allow for better reproducibility and comparability of the measured particle concentrations but was recognized too late during the experiment.

Table 3: Uncertainties of the used measurement instruments obtained from the respective manuals [46], [50], and [47].

Instrument	**Uncertainty**
FCE (TSI 3068)	± 2% of the measured current (at least ± 5 fA)
Flowmeter (TSI Series 4100)	± 2% of the measured flow rate (at least 0.05 lpm)
Tube Furnace (Carbolite Gero EHA Model)	Temperature accuracy is not stated in the manual. Temperature values are assumed to be free of uncertainty.

4 Experiment and Results

At the beginning of every measurement day, the flow rates were checked and (if necessary) readjusted to 1.4 lpm through the tube furnace and 2.8 lpm through the DMA. The sheath flow was checked to be even and at a rate of 18.5 lpm within the measurement accuracy of the flowmeter of 2 %. For the FCE, a zero offset reset was performed every morning with a HEPA-filter and the thermostat was set to 15 °C (except for one measurement in which the influence of the cooling temperature was investigated). Finally, before beginning the measurements, the FCE signal without a sample was checked to rule out any contaminations of the furnace tube, the tubing between furnace and FCE, or the DMA. If necessary, the setup was cleaned and baked out as described in 4.5.4 "Plastic Contamination of the Experimental Setup". The following pages show the insights and results acquired from this experiment.

4.1 Sample Morphology During Heating

As discussed in chapter 2.1 "What is Plastic?", all three examined plastic types are semi-crystalline thermoplastics, meaning they melt upon heating and harden out again upon cooling. To find out the melting temperatures of the used plastics, the samples were heated in increasing 10 °C steps. The observed melting points of the samples were around 15 °C to 20 °C higher than the literature values listed in the theory chapters of LDPE, PP, and PET. This is likely because not the sample temperature, but the furnace temperature was measured, with the samples themselves being exposed to a cooling air stream through the furnace glass tube. Furthermore, the melting point of the samples during this experiment was defined as the temperature at which the plastic was completely molten. The onset of the melting process can already be observed at slightly lower temperatures with the plastic flakes not being completely molten but starting to stick together. Lastly, the literature values for the melting temperatures of LDPE, PP, and PET are given for additive-free polymers, whereas the samples used during this experiment are everyday plastic items, that likely contain various additives and a mixture of different tacticities in the case of PP. **Table 4** shows the observed melting points and the morphological changes of the samples during the experiment.

Table 4: Observed melting temperatures and morphological changes during heating of the examined LDPE, PP, and PET samples.

	LDPE	**PP**	**PET**
Observed melting temperature	≈ 130 °C	≈ 180 °C	≈ 270 °C
Morphological changes during heating	melting, brown discoloration	melting, change from translucency to transparency, slight brown discolorations	curling of flakes, melting, brown discoloration

At which temperatures the plastic samples start to show deformations and discolorations depends on the type of plastic as well as the amount of time the samples are exposed to said temperatures. **Figure 20** shows the three different plastic samples after being heated to 200 °C for around 90 minutes. LDPE and PP were molten completely with LDPE starting to show slight yellowish-brown discolorations. With PET having the highest melting point of the three samples, its flakes were not molten at 200 °C but started to curl and deform.

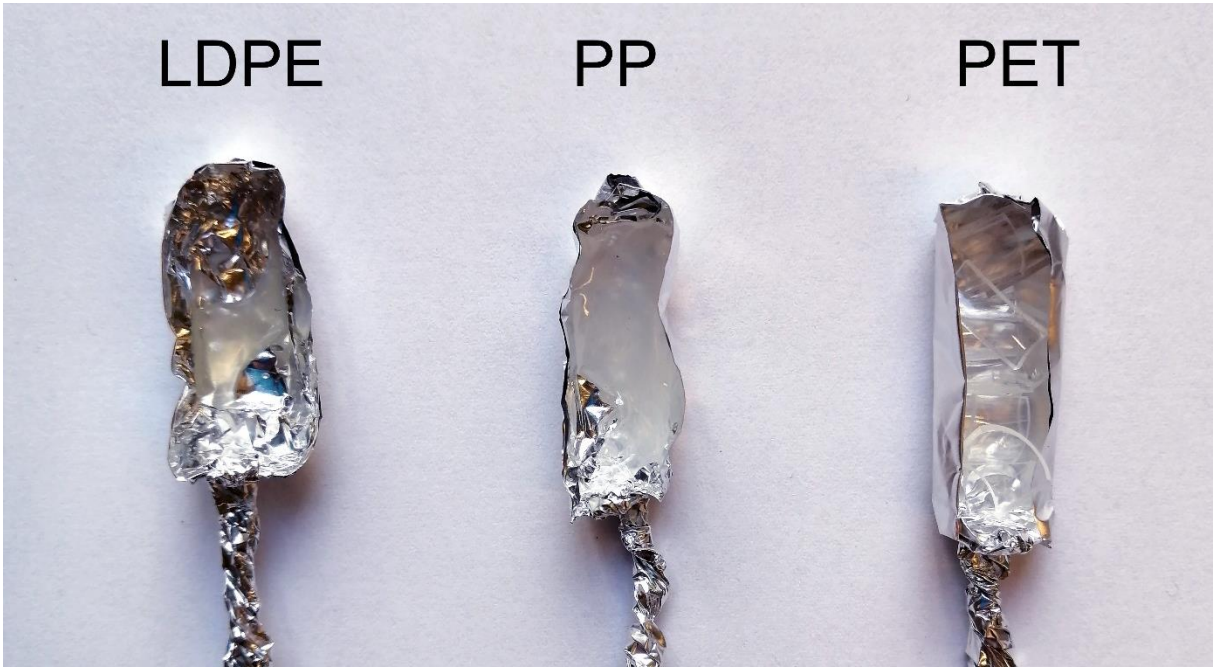

Figure 20: LDPE, PP, and PET samples after being heated at 200 °C for approximately 90 minutes.

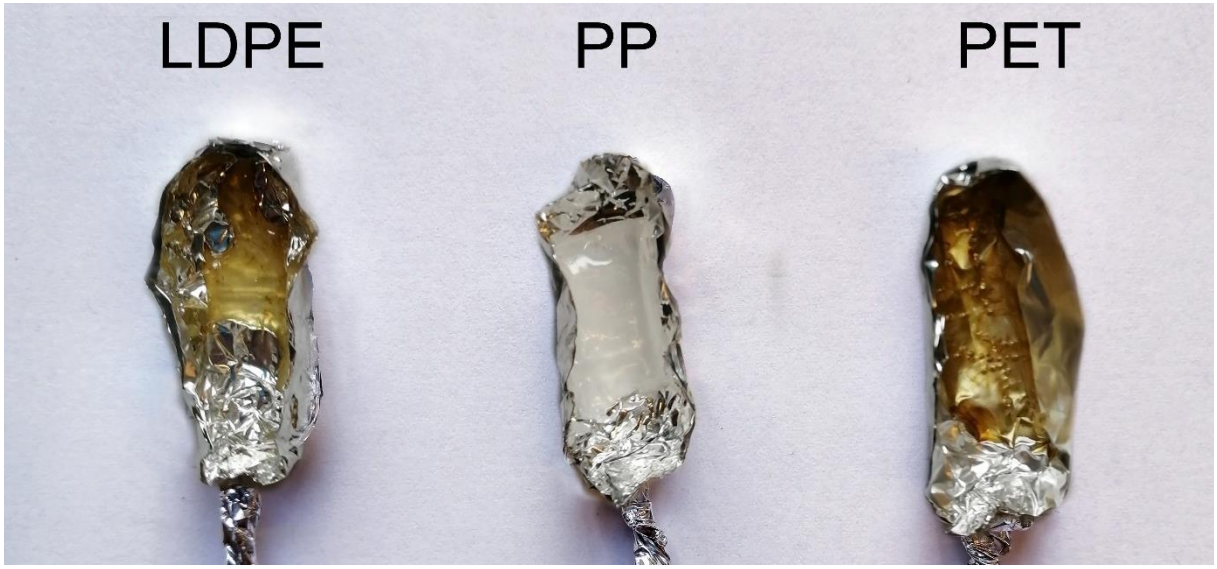

Figure 21: Plastic samples after gradually being heated to 150 °C (LDPE), 140 °C (PP), and 310 °C (PET).

Figure 21 shows the three plastic types after being gradually heated from 150 °C to 250 °C for LDPE, from 140 °C to 240 °C for PP, and from 180 °C to 310 °C for PET. The temperature was incremented in 10 °C-steps and each temperature was held for approximately 10 minutes in accordance with the temperature profiles done for **Figure 22**. All samples were completely molten, and LDPE and PET showed clear brown discolorations. The PP sample also showed slight brownish discolorations of smaller plastic droplets on the sides of the aluminum spoon. In comparison to the other two plastic types, the discolorations were very small and therefore, they are not visible in **Figure 21**. Initially, it was not clear, whether these discolorations stem from additives or thermal-oxidative degradation of the plastic samples. In the former case, additives like plasticizers or flame retardants could have diffused to the surface during heating and formed a layer on top of the molten plastic, as observed by Wei et al. (2019) and discussed in chapter 2.1.2 “Chemical Additives”. With the applied temperatures being close to the thermal-oxidative degradation temperatures found by Sudip and Cooney (2018) for LDPE, PP, and PET, the discolorations could also result from an on-setting degradation of the polymers. As the three examined additive-free polymers showed the same brownish color after heating as the commodity plastics, at least part of the discolorations likely stem from polymer degradation. However, this does not explain why LDPE shows much more and earlier discolorations as PP, although according to Sudip and Cooney (2018) the two plastic types have the same thermal-oxidative degradation temperature and PP degrades faster than LDPE once degradation is triggered [51]. Furthermore, PET shows the highest degree of discoloration of all three samples, although it was furthest from reaching its degradation temperature.

While PP exhibited the smallest amount of discoloration, it showed the clearest transition between transparency and translucency. Right after removing the spoons from the furnace, the PP samples were completely clear and transparent, almost invisibly so. Only upon cooling, they became the white translucent color seen in the image above. This is likely the result of the PP sample being completely amorphous and therefore transparent in its molten form but partially recrystallizing and becoming translucent upon cooling, as discussed in chapter 2.1.1.1 “Crystallinity, Branching, and Crosslinking”. This is interesting, as the PP flakes were transparent before heating. Possibly, the degree of crystallinity is purposefully controlled during the manufacturing of plastic goods to obtain transparency. Beneath the discolorations of the LDPE and PET samples, the degree of transparency is less evident. Upon close examination and disregarding the brown discoloration, PET retains most of its transparency, while LDPE seems to be more translucent, albeit less so than PP.

4.2 Temperature Profiles of Commodity LDPE, PP, and PET

Before attempting to record individual number size distributions, it was first necessary to find out, if and at which temperatures nanoparticles can be generated from the different samples. This was done by measuring temperature profiles of the three examined plastic types. Starting at 80 °C and increasing the temperature in 10 °C-steps in between runs, one EMS run was recorded at each temperature to see, if a peak could be measured. The onset of particle emission was observed at around 160 °C for LDPE, 150 °C for PP, and 180 °C for PET. **Figure 22** shows the temperature profiles obtained from these measurements. The lower temperature ranges, in which no particles were measured, are not pictured. While there is a minimum temperature for nanoparticle generation from heated plastic, there does not seem to be a maximum temperature. Particle concentrations increased at every temperature step for all three plastic types. Therefore, the high ends of the temperature profiles were not chosen because of decreasing particle concentrations but because of methodological reasons, as at high temperatures the plastic becomes liquid enough to leak from the aluminum foil spoons and contaminate the furnace tube. It should be noted, that the temperature profiles in **Figure 22** are likely understating the measured temperatures by a few °C, as the used tube furnace takes some time to stabilize at a certain temperature and overheats by a few °C when heated to a new temperature. For example, a small PP peak was measured at (nominal) 150 °C during the temperature profile measurements, while no peak was observed when giving the furnace time to stabilize at the set temperature before inserting the sample. Increasing the temperature to (stable) 160 °C resulted in the anticipated peak.

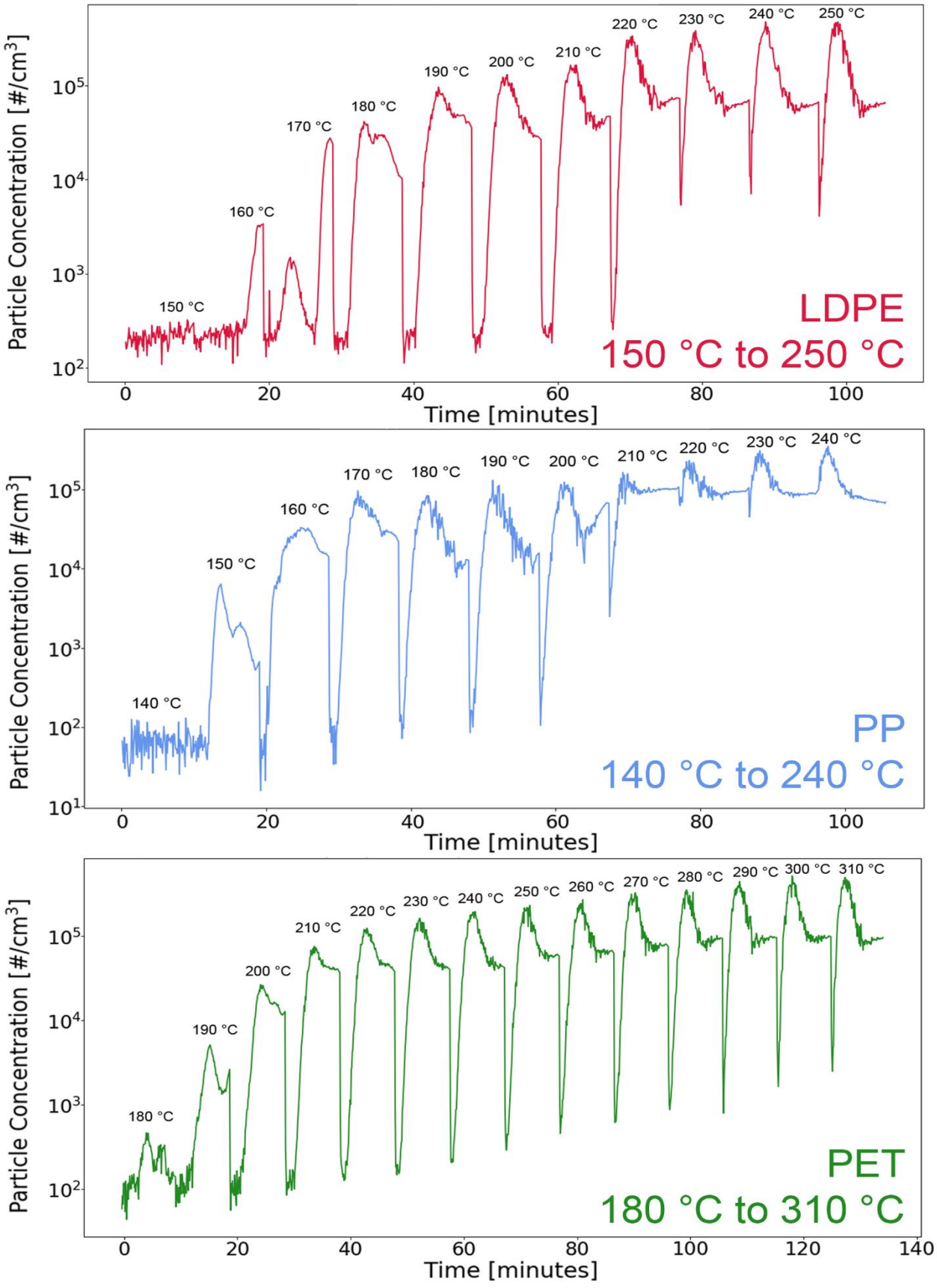

Figure 22: Temperature profiles of LDPE, PP, and PET. At each temperature, a full EMS run was done to obtain a size distribution peak.

4.2.1 Temperature Dependence of Maximum Particle Concentration

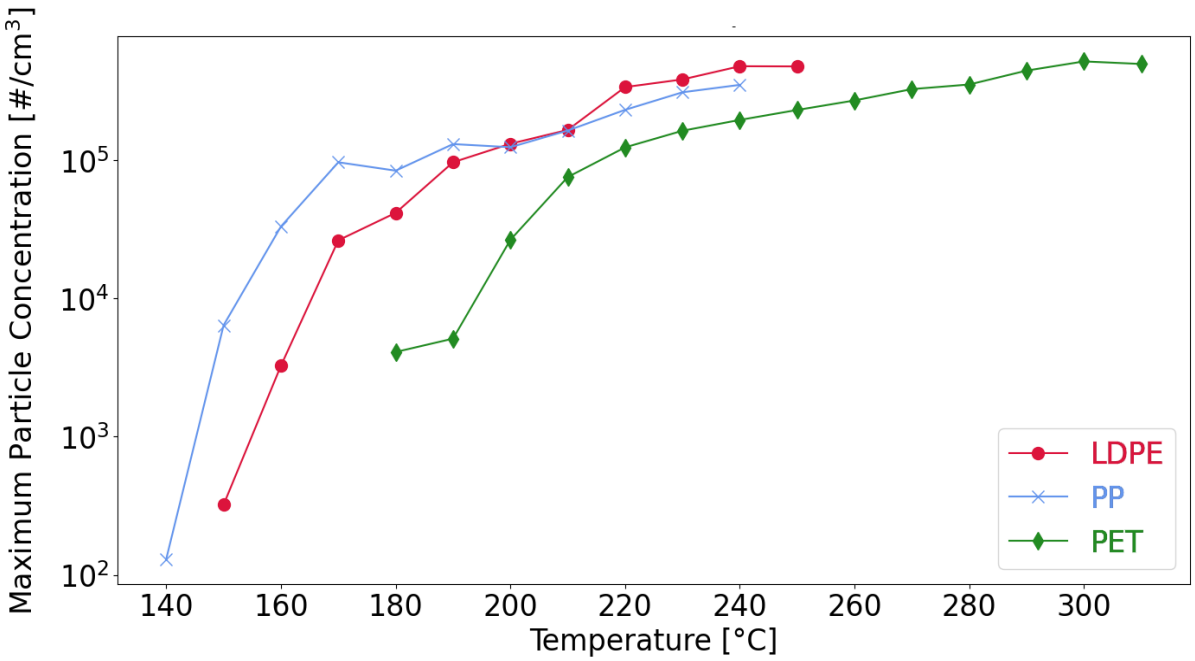

Figure 23: Maximum particle concentration versus temperature for LDPE (red), PP (blue), and PET (green).

Figure 23 shows the maximum particle concentration measured at each temperature step of the temperature profiles for LDPE, PP, and PET. The maximum concentrations increase with increasing temperature for all three plastic types and seem to converge towards an upper limit in the order of 10^5 particles/cm^3. Except for LDPE between 240 °C and 250 °C, the same was found in the more precise number size distribution measurements in the following chapter. For reasons of consistency with the temperature profiles in the previous subchapter, the data points for PP at 140 °C and LDPE at 150 °C were included in **Figure 23** and **Figure 24**, although no distinct peaks were measured at these temperatures for the respective plastic types.

4.2.2 Temperature Dependence of Electrical Mobility Diameter

Figure 24 shows the mode electrical mobility diameter of the size distributions obtained at each temperature step of the temperature profiles above. Like the maximum concentrations, the mode mobility diameters generally increase with increasing temperature. However, the trend is less distinct (except for PET). The same was found in the number size distribution measurements shown in the following chapter, where the measured mode mobility diameters increased with temperature for PP and PET but showed no clear pattern for LDPE.

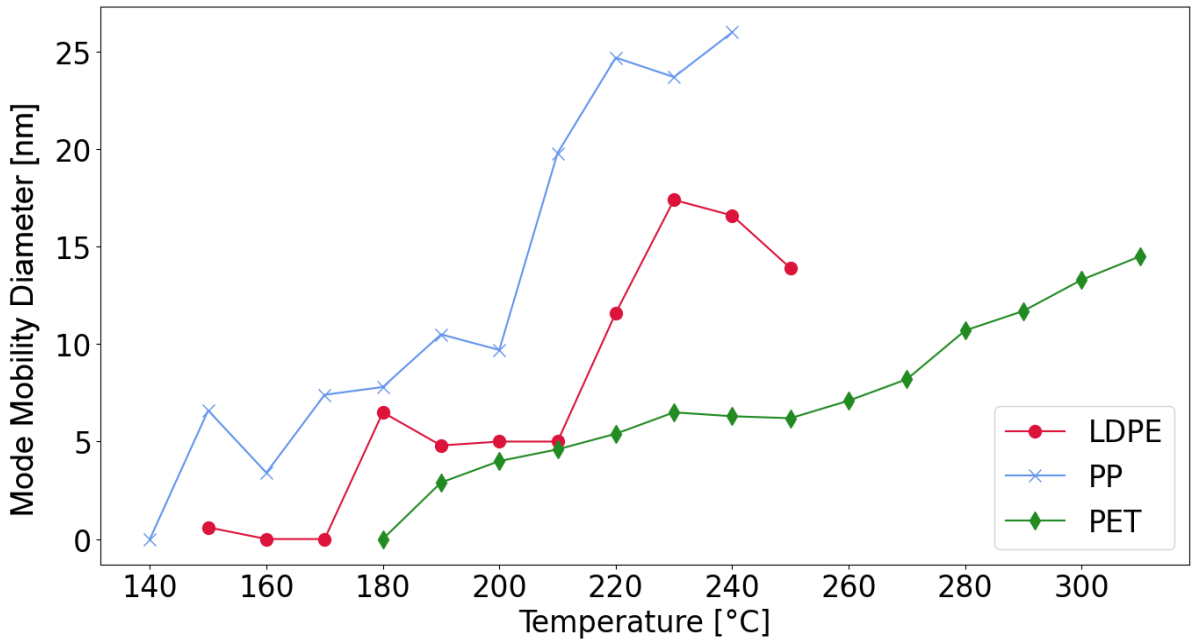

Figure 24: Mode electrical mobility diameter versus temperature for LDPE (red), PP (blue), and PET (green).

4.3 Number Size Distributions of Commodity Plastics

The temperature profiles in the previous chapter already show that the shape of the peaks measured during the experiment changes with temperature. To quantify this effect, number size distributions at four different temperatures were recorded for each of the three considered commodity plastic types. As not all temperatures seen in the temperature profiles produce stable particle peaks when measured over a longer time, the first step was to find a minimum temperature for each plastic type, above which the recorded peaks were stable long enough to make multiple measurements of the same peak. For LDPE this temperature was found to be 220 °C, for PP 190 °C, and for PET 260 °C. The number size distributions shown in the following plots are the average of 10 EMS runs per temperature and plastic type. To characterize the number size distributions, the peaks were fitted with a log-normal distribution using the program Fityk [49]. The maximum particle concentrations, mode electrical mobility diameters (in the following pages shortened to “mobility diameter” or “mode diameter”), and full-width-half-maximum (FWHM) values of these fitted curves are listed in the tables below the respective plots. The uncertainty values were calculated as discussed in chapter 3.4 “Uncertainty Estimation”.

4.3.1 Commodity LDPE

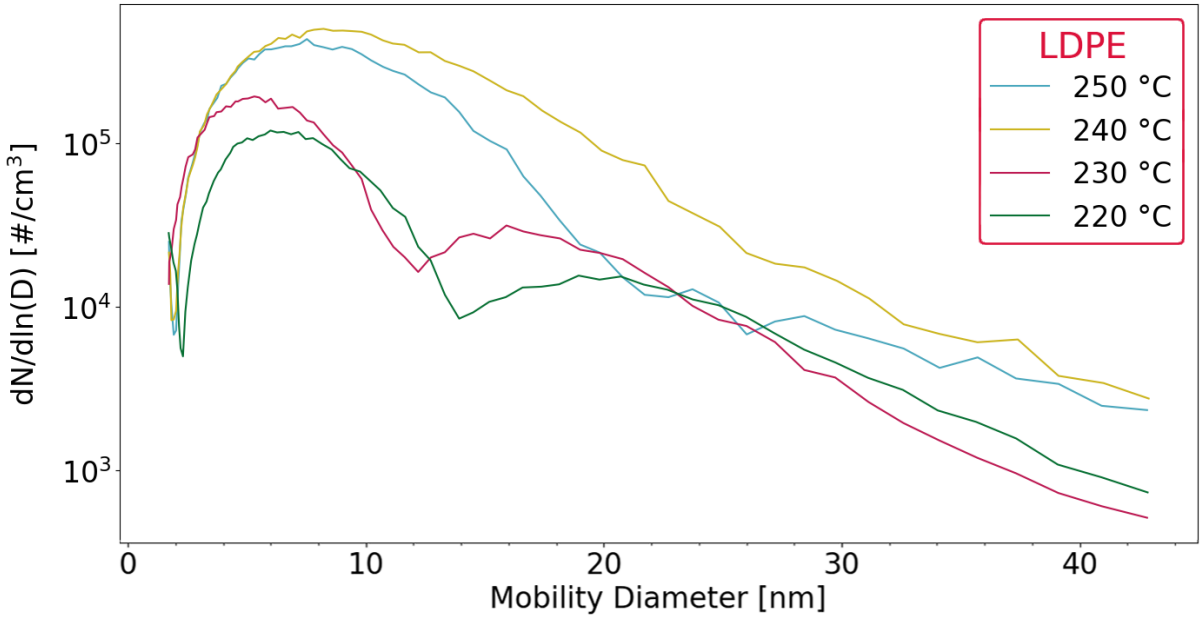

Figure 25: Number size distributions of commodity LDPE at different temperatures.

Figure 25 shows the number size distributions of commodity low-density polyethylene measured in the temperature range from 220 °C to 250 °C. At 220 °C and 230 °C, the distributions show double peaks. As discussed in chapter 4.4 "Additive-Free Polymers Versus Commodity Plastics", likely only one of them stems from the polymer itself. A possible explanation for the additional peak is the presence of additives in commodity LDPE, which might evaporate from the plastic and appear as a secondary particle peak in the plot. The double peaks were fitted with two log-normal distributions, the peaks at 240 °C and 250 °C with one log-normal distribution, respectively. The characteristics of the number size distributions shown in **Figure 25** are listed in **Table 5** below.

Table 5: Characteristics of the LDPE number size distributions from **Figure 25**.

Temperature [°C]	Maximum Particle Concentration(s) [#/cm³]	Mode Diameter(s) [nm]	FWHM [nm]
250	426,500 ± 9,200	7.0 ± 1.1	7.7 ± 2.1
240	505,000 ± 11,000	8.0 ± 1.2	9.6 ± 2.4
230	197,800 ± 4,400 27,900 ± 1,400	5.12 ± 0.77 16.4 ± 2.5	5.3 ± 1.5 7.8 ± 4.9
220	123,500 ± 2,800 14,700 ± 1,400	6.27 ± 0.94 19.5 ± 2.9	5.9 ± 1.9 9.8 ± 5.9

4.3.2 Commodity PP

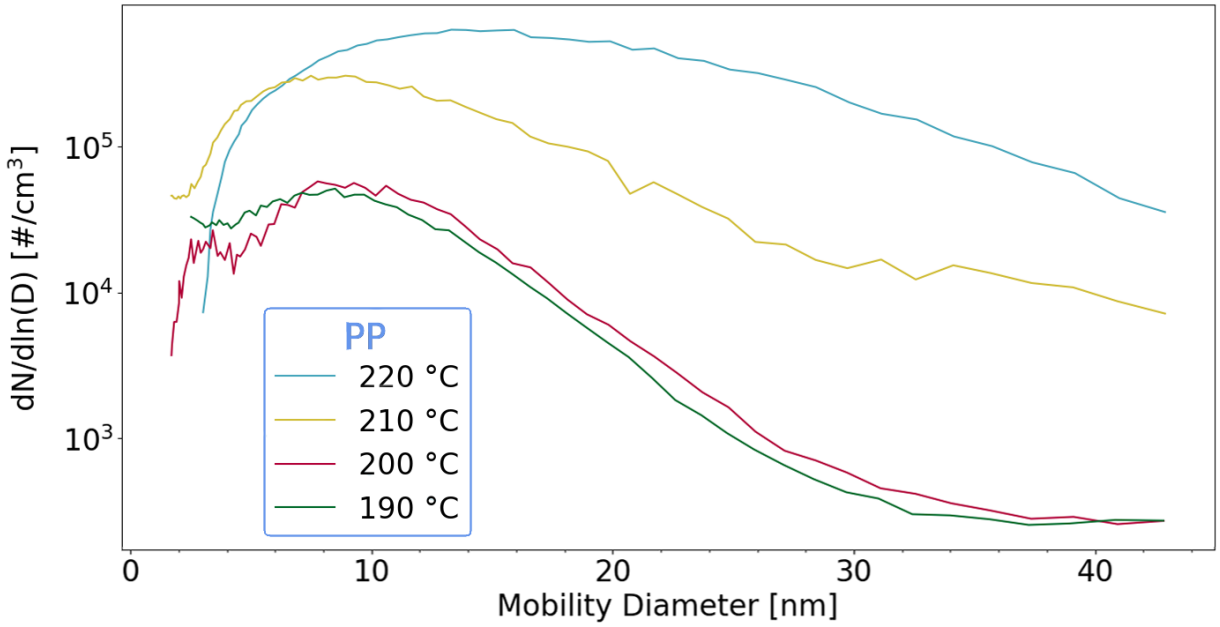

Figure 26: Number size distributions of commodity PP at different temperatures.

Figure 26 shows the number size distributions of commodity polypropylene measured in the temperature range from 190 °C to 220 °C. It should be noted, that the curves at 210 °C and 220 °C were recorded during additional measurements with a new PP sample, and maximum particle concentrations of the 190 °C to 200 °C and the 210 °C to 220 °C temperature ranges are therefore not directly comparable. Nevertheless, the maximum particle concentrations increase steadily with temperature. This is apparent from the number size distribution characteristics listed in **Table 6**, alongside with the corresponding mode diameters and FWHM values. Contrary to LDPE and PET, PP did not show double peaks at any of the measured temperatures.

Table 6: Characteristics of PP number size distributions from **Figure 26**.

Temperature [°C]	Maximum Particle Concentration [#/cm³]	Mode Diameter [nm]	FWHM [nm]
220	648,000 ± 14,000	13.6 ± 2.0	16.8 ± 4.1
210	296,500 ± 6,500	8.3 ± 1.2	11.1 ± 2.5
200	51,800 ± 1,500	9.2 ± 1.4	9.3 ± 2.7
190	47,000 ± 1,500	7.8 ± 1.2	10.3 ± 2.3

4.3.3 Commodity PET

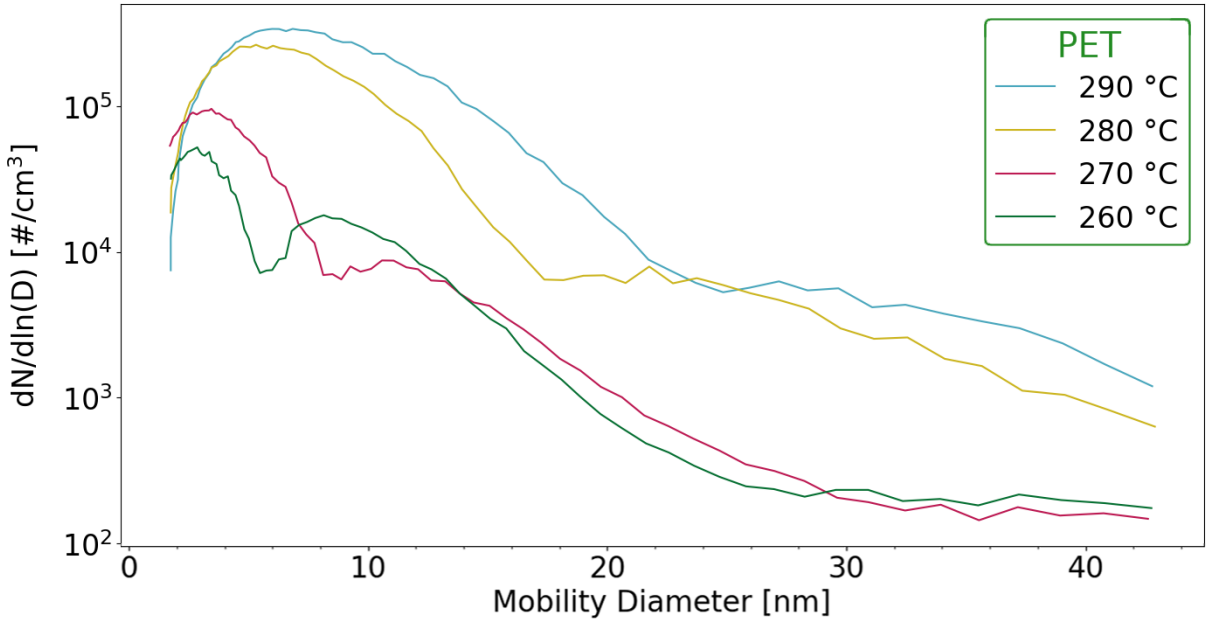

Figure 27: Number size distributions of commodity PET at different temperatures.

Figure 27 shows the number size distributions of commodity polyethylene terephthalate measured in the temperature range from 260 °C to 290 °C. Like LDPE, PET shows double peaks at lower temperatures, most prominently at 260 °C. Of all three considered plastic types, PET number size distributions behave the most predictable. Mode particle concentrations, mode diameters, and FWHM values increase steadily with temperature, as can be seen in **Table 7**.

Table 7: Characteristics of PET number size distributions from **Figure 27**.

Temperature [°C]	Maximum Particle Concentration(s) [#/cm³]	Mode Diameter(s) [nm]	FWHM [nm]
290	353,100 ± 7,600	6.29 ± 0.94	7.5 ± 1.9
280	270,400 ± 5,900	5.42 ± 0.81	6.2 ± 1.6
270	93,100 ± 2,200 7,600 ± 1,300	3.17 ± 0.48 11.0 ± 1.6	3.90 ± 0.95 5.3 ± 3.3
260	49,800 ± 1,500 17,600 ± 1,400	2.75 ± 0.41 8.2 ± 1.2	2.86 ± 0.82 5.0 ± 2.5

4.4 Additive-Free Polymers Versus Commodity Plastics

The focus of this thesis lies on everyday plastic items (here called commodity plastics), as they have the highest environmental significance. However, comparison measurements were made with additive-free versions of LDPE, PP, and PET. The high-purity polymers were bought from Sigma-Aldrich and have the respective CAS numbers 9002-88-4 (LDPE), 9003-07-0 (isotactic PP), and 25038-59-9 (PET). The additive-free polymers start to produce nanoparticles at roughly the same temperatures as their commodity counterparts. One temperature was chosen for each plastic type to showcase the differences between the number size distributions produced by additive-free plastic and commodity plastic. A new quartz glass tube, a new cooling tube, and new glass spoons wrapped in aluminum foil were used for the measurements.

All three additive-free polymers produced nanoparticles in a similar way as their respective commodity plastic variants. Hence, it is justified to refer to the aerosols generated for this thesis as "nanoplastic aerosols", as at least part of the observed aerosol particles stem from the polymer itself. Interestingly, the additive-free polymers produced the most similar peak shapes in comparison to the commodity plastics when heated at 10 °C higher temperatures. **Figure 28** shows the comparison of the additive-free polymer number size distributions versus the commodity plastic number size distributions for LDPE, PP, and PET. Why the additive-free polymers need 10 °C higher temperatures to produce nanoparticles in the same way as their commodity variants is not immediately clear from the experiment. A possible explanation could be, that the additive-free polymers likely exhibit a higher degree of crystallinity, as there are no additive molecules that disturb the crystal structure. As described in chapter 2.1.1 "Chemical Structure of Plastics", a higher degree of crystallinity increases the melting point and could therefore explain the observed temperature effect. **Table 8** below the figure lists the maximum particle concentrations, mode diameters, and FWHM values of the additive-free and commodity plastic number size distributions shown in **Figure 28**.

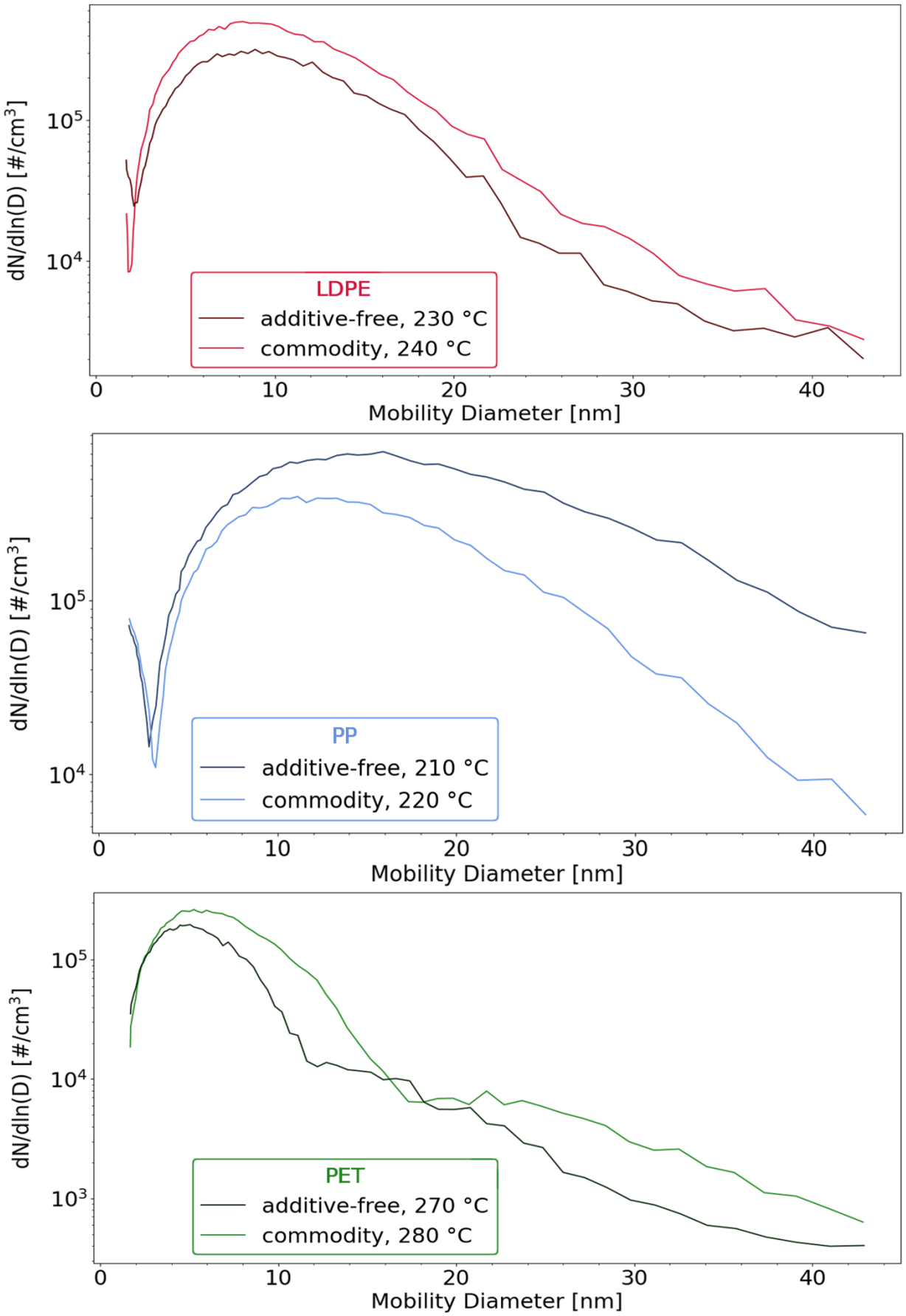

Figure 28: Number size distributions of additive-free polymers (dark lines) and commodity plastics (light lines) for LDPE (red), PP (blue), and PET (green).

Table 8: Characteristics of additive-free and commodity plastic number size distributions from **Figure 28**.

Plastic Type, Temperature	Maximum Particle Concentrations [#/cm^3]	Mode Diameters [nm]	FWHM [nm]
additive-free LDPE, 230 °C commodity LDPE, 240 °C	313,200 ± 6,800 505,000 ± 11,000	8.5 ± 1.3 8.0 ± 1.2	10.0 ± 2.5 9.6 ± 2.4
additive-free PP, 210 °C commodity PP, 220 °C	405,100 ± 8,700 648,000 ± 14,000	12.0 ± 1.8 13.6 ± 2.0	13.7 ± 3.6 16.8 ± 4.1
additive-free PET, 270 °C commodity PET, 280 °C	194,500 ± 4,300 270,400 ± 5,900	4.61 ± 0.69 5.42 ± 0.81	5.3 ± 1.4 6.2 ± 1.6

When compared at the same (and slightly lower) temperature, another difference between additive-free polymers and commodity plastics becomes apparent. Commodity LDPE and PET both show distinct double peaks at some temperatures, while their additive-free versions only form one peak at all measured temperatures. This effect is shown in **Figure 29** for the case of LDPE at 230 °C. This suggests, that only one of the peaks in the number size distribution of commodity LDPE shows actual nanoplastic particles, while the second peak is likely produced by additives. It is not clear from this experiment if this is indeed the case and if so, which peak is which. To find out, further investigations (for example with a mass spectrometer) would be necessary.

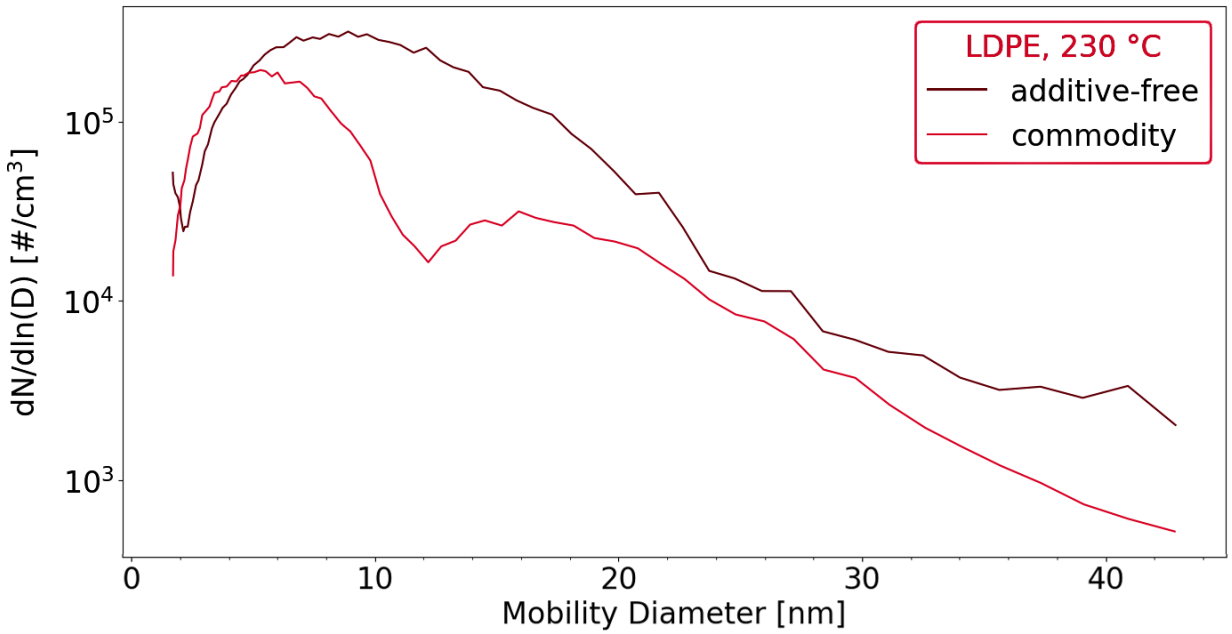

Figure 29: Number size distributions of additive-free LDPE (dark red) and commodity LDPE (light red) at 230 °C.

4.5 Miscellaneous Findings and Troubleshooting

This short chapter lists insights acquired during the experiment that are not directly related to the research question but might still be interesting for researchers looking to recreate the experiment. Special consideration should be given to 4.5.4 “Plastic Contamination of the Experimental Setup”, as the therein discussed contaminations have proved to be inevitable during the experiment.

4.5.1 Unstable Particle Concentrations

In some instances, it was observed, that measured particle concentrations decreased significantly or disappeared altogether while measuring over longer periods at the same temperature. An example is PET at 200 °C, as can be seen in **Figure 30**. This usually means that the chosen temperature is too low to produce stable particle concentrations. Even if the measured concentrations drop to zero, it is often enough to increase the temperature by 10 °C or 20 °C to reobtain and stabilize concentrations peaks from the same sample. PET produces stable particle concentrations from 260 °C upwards, LDPE from 220 °C upwards, and PP from 190 °C upwards. At these temperatures, no noticeable drop in particle concentration could be observed.

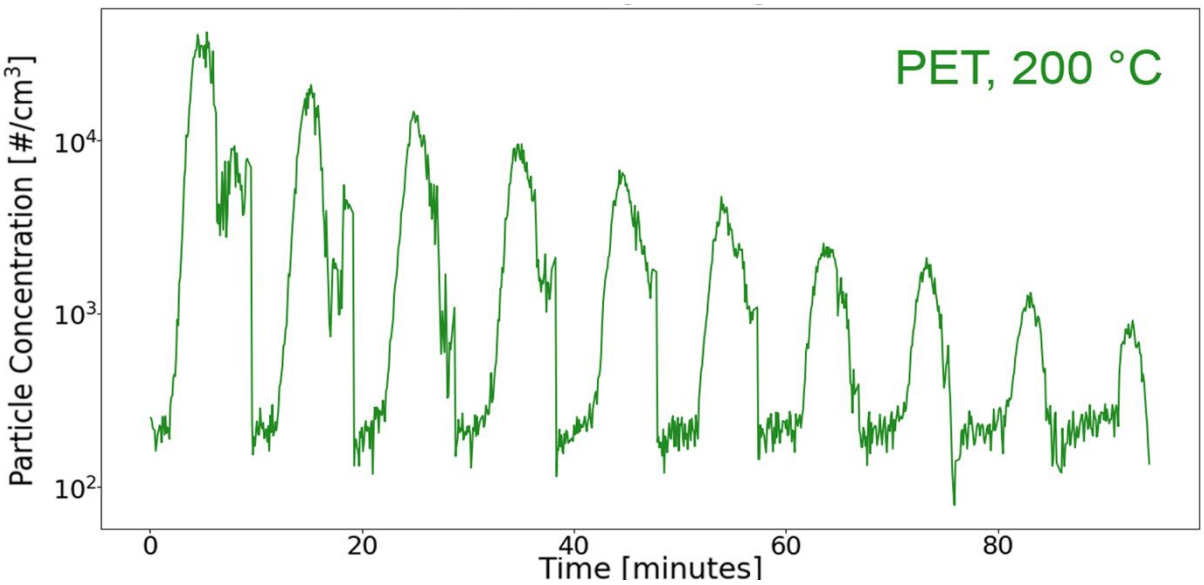

Figure 30: Waning particle concentrations of PET at 200 °C over time.

More unexpectedly, the particle concentrations may also increase over time. This has only been observed for commodity LDPE and is likely due to diffusion-controlled evaporation of additives, as introduced by Wei et al. (2019) and discussed in chapter 2.1.2 "Chemical Additives". As it takes some time for the additives to reach the plastic surface, lower concentrations are observed at first. After enough additives have diffused to the surface to sustain continuous evaporation, the particle concentrations stabilize.

4.5.2 Reusing Old Samples

It was investigated if a sample could be reused the following day, even if the (in most cases) molten plastic solidified overnight. For all three plastic types, it was possible to generate nanoparticles from old samples. **Figure 31** shows size distributions of PP at 200 °C measured on two consecutive days with the same sample. The curves coincide within the measurement uncertainties for mobility diameters greater than 7 nm. Below 7 nm, the old sample showed slightly lower particle concentrations. The waning particle concentrations of PET at 200 °C seen in the previous chapter continued to drop the following day until no peaks could be observed. The only sample that showed a significantly different behavior after being cooled down and reheated the next day was LDPE. Here, the old sample showed higher particle concentrations, up to a factor of 10. Additionally, waning peaks of the new LDPE sample were perfectly stable for the same sample at the same temperature the next day. As above, diffusion-controlled evaporation of additives could explain this phenomenon.

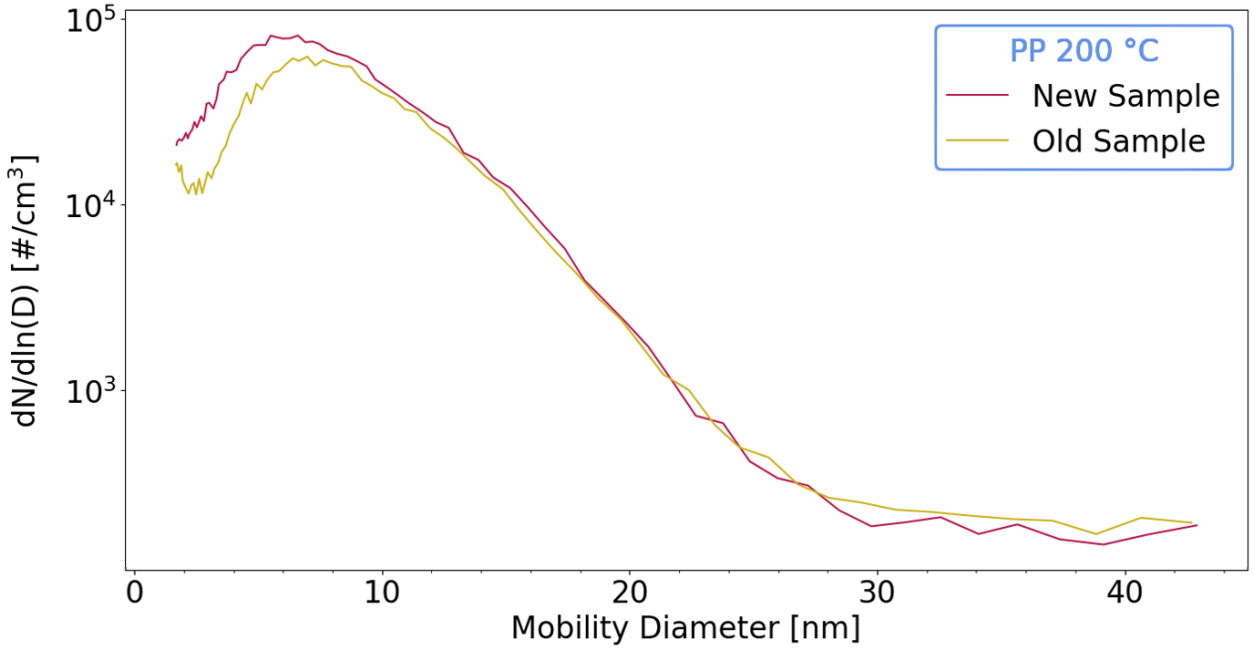

Figure 31: Comparison of the same PP sample at 200 °C on two different days.

4.5.3 Effect of Cooling Temperature After the Furnace

To assess the effect of the cooling temperature after the furnace, peaks for PP at cooling temperatures of 25 °C, 20 °C, 15 °C and 10 °C were measured. The furnace temperature was set to 220 °C in all four measurements. As can be seen in **Figure 32**, the distributions shift to slightly smaller diameters for lower cooling temperatures. However, the overall effect is small, especially at mobility diameters below 20 nm. In all measurements besides the ones in **Figure 32**, a cooling temperature of 15 °C was used. Without any cooling at all, high concentrations of particles are still measured but they do not form peaks as seen above, indicating that particles nucleate directly from the vapor phase when cooled. This was tested with pure PP, where the furnace tube was directly connected to the charger and the DMA without intermediate cooling.

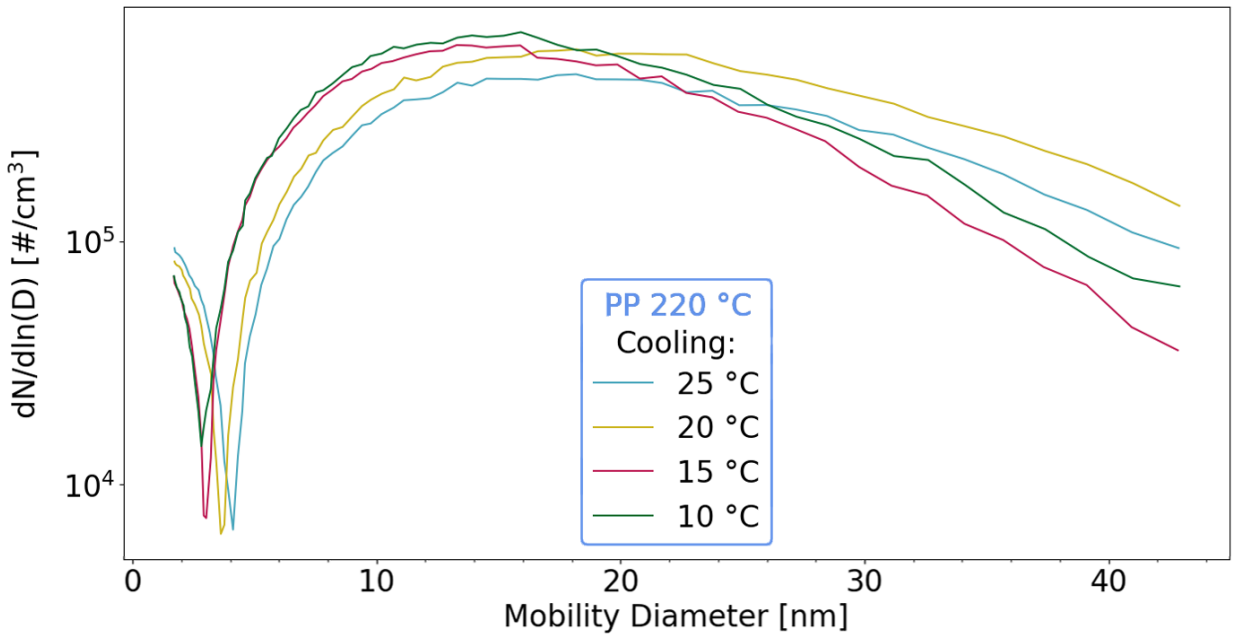

Figure 32: Effect of cooling temperature on PP at a furnace temperature of 220 °C.

4.5.4 Plastic Contamination of the Experimental Setup

During the experiment, special attention must be paid to possible plastic contaminations of the experimental setup. The FCE background was checked before every measurement and if necessary, the tubing, DMA, or furnace glass tube cleaned and baked out. To prevent molten plastic from sticking to glass spoons and therefore making them unusable, spoons made from aluminum foil were used. Twice during the beginning of the experimental phase, the DMA as well as the entire tubing section between furnace and FCE had to be cleaned. Small, black rubber flakes were found inside the tubing and the DMA, leading to high background measurements of the FCE without an inserted sample. In both cases, this has happened with a thin LDPE foil at around 220 °C. By switching to a slightly thicker LDPE foil, the problem could be resolved. Besides preventing irreversible contamination, aluminum foil spoons are better than glass spoons for this specific problem, as they can be folded as needed to prevent larger plastic flakes from being blown out of the spoon.

Most common, however, are contaminations of the furnace glass tube. In one instance during the beginning of the experiment, LDPE seemed to start boiling and was later found sticking to the top of the glass tube. At this time, a glass spoon was still used, and it could only be taken out by heating the tube to around 200 °C to liquefy the plastic enough to free the spoon. For this reason, it is advised not to fill the spoon completely with plastic but to leave enough room for melting and possibly boiling plastic. Moreover, if the plastic becomes too hot, it

liquefies enough to leak from the aluminum foil spoons. Finally, samples need to be inserted very carefully. If one of the commodity plastic flakes or additive-free polymer granules falls out of the spoon during sample insertion at high enough furnace temperatures, it will almost immediately melt and stick to the glass tube. When this happened, the glass tube was cleaned by scratching out the remaining plastic as well as possible and then washed out with water. After that, the tube was baked out at 300 °C for about an hour. In all cases, this brought the measured particle background back to normal levels. As can be seen in **Figure 33**, the contaminations in the furnace glass tube show the same brown discolorations as the plastic samples at high temperatures. With each baking-out the color gets darker, indicating more and more degradation.

Figure 33: Contaminated furnace glass tube after the end of the experiment.

5 Discussion and Conclusion

"Can airborne nanoparticles be generated by heating plastic?" – yes, they can. Airborne nanoparticles can be generated by heating from all three investigated plastic types LDPE, PP, and PET. They can also be generated in the same way from their respective additive-free versions, warranting the restatement of the research question in its original form: "Can airborne *nanoplastics* be generated by heating plastic?". This was not immediately clear, as commodity plastics contain an (in most cases undeclared) variety of additives that could evaporate during heating and show up as nanoparticles during measurements. By showing that additive-free polymers produce aerosols in a similar way as their everyday-use counterparts, it was established, that at least some of the measured particles truly stem from the polymer itself and the generated aerosols can therefore be referred to as "nanoplastic aerosols". However, double peaks in the number size distributions of commodity LDPE and PET at some temperatures indicate, that the generated aerosols contain nanoplastic *and* additive particles.

Although the term "nanoplastic" encompasses the relatively large size range of 1 nm to 1000 nm, only a small part on the lower end of this size range was considered. The Vienna-type nano-DMA and the FCE used for the experiment allowed for measurements in the size range of approximately 2 nm to 45 nm. The generated aerosols showed mode electrical mobility diameters in the range of approximately 3 nm to 20 nm, with the majority lying between 6 nm and 8 nm. Comparing these results with Pitt et al. (2017) and Mattsson et al. (2017), who studied the uptake of polystyrene particles with diameters of up to 53 nm by fish, suggests, that the generated aerosol particles are small enough to enter organs and pass through the blood-brain-barrier. In accordance with Hollóczki and Gehrke (2019), they might even be small enough to penetrate cellular membranes and lead to cell death.

The temperatures at which the three considered plastic types start to produce nanoparticles were found to be around 160 °C for LDPE, 150 °C for PP, and 180 °C for PET. An upper temperature limit for the production of aerosol nanoparticles from heated plastics could not be found due to experimental limitations. Generally, particle number concentrations steadily increased up to the highest measured temperatures (250 °C for LDPE, 240 °C for PP, and 310 °C for PET) and likely continue to increase with temperature until the samples decompose significantly. Based on the found particle generation onset temperatures, it is unlikely that airborne nanoplastics are formed during activities such as cooking or cleaning. A possible exception could be silicone, a polymer that is often used in baking dishes or oven

gloves, but which was not considered during this experiment. A more likely source of airborne nanoplastics is waste incineration plants, which are required to reach at least 850 °C for two seconds. It cannot be stated from this experiment if plastics continue to produce airborne nanoparticles at such high temperatures. However, as plastic waste is heated to reach 850 °C, aerosol nanoplastics likely form in the same way as they did in this experiment. The question remains, how fast waste is heated in such incineration plants and how much time the plastics have to emit nanoparticles. Nevertheless, this thesis supports the idea by Dris et al. (2016), who believe waste incineration plants to be a possible source of airborne micro- and nanoplastics. As recently shown by Yang et al. (2020), microplastics can still be found in the bottom ash of waste incineration plants. With this knowledge and the findings of this thesis, it seems reasonable to assume, that flue gasses produced by waste incineration plants also contain plastic particles. The small particle sizes found during this experiment make it easy to imagine that some of these flue gas nanoplastics might escape filtration and get emitted into the atmosphere. As PP started to emit nanoparticles close to its melting temperature and PET even considerably below its melting temperature, another source of airborne nanoplastics could be the plastics processing industry. Processes like injection molding or extrusion use molten polymers to produce plastic items from polymer granules or powders. Workers in these industries could be subject to negative health effects by inhaling nanoplastics generated during this polymer processing in a similar way as Prata et al. (2018) found that synthetic textile and flocking workers are at a higher risk of developing respiratory occupational diseases due to the inhalation of microplastics.

6 Future Research

While writing this thesis, many interesting questions came to mind that would be worth studying. Within the limitations of a master's thesis, only a few could be addressed, leaving the rest of them – as exciting as they may sound – to the realm of speculation. Nevertheless, I chose to dedicate this short chapter to those questions, in hope someone might read and find them interesting enough to study them.

As the title of this thesis states, only nanoparticles were investigated. Microplastics were not considered, although the formation of microplastics through agglomeration of nanoplastics would be imaginable. This would be interesting in the sense that usually only the degradation from micro- to nanoplastics is considered but not the possible formation of microplastics through clustering of nanoplastics. The question, thus, is:

"Can microplastics form through agglomeration of nanoplastics?"

Secondly, one does not come far in the field of aerosol physics without coming across the study of cloud formation. As mentioned in the introduction of this thesis, the potential of micro- and nanoplastics as ice nuclei was already shown by Ganguly and Ariya (2019). It would be interesting to see, if nanoplastics also act as cloud condensation nuclei (CNN) and which sizes, shapes, and chemical compositions of plastic particles would make a "good" CNN. The question reads:

"Under which circumstances could nanoplastics act as cloud condensation nuclei?"

Lastly, a morphological study of the generated aerosol particles could be undertaken. It would be thinkable, that different temperatures and plastic types produce different nanoparticle shapes and therefore also different behavior in the environment and the human body. It would be highly interesting to see an electron microscope picture of the nanoparticles created during this experiment and whether or not temperature or plastic type play a role in the shapes created. The questions are:

"What particle shapes are created during the generation of nanoplastic aerosols?"

"What influence does temperature and plastic type have?"

Should any or all of these questions ever be answered, I hope that the results of their studies find their way to me.

7 Closing Remarks

I would like to end this thesis with the same quote with which it began:

> *"Aristotle said a bunch of stuff that was wrong. Galileo and Newton fixed things up. Then Einstein broke everything again. Now, we've basically got it all worked out, except for small stuff, big stuff, hot stuff, cold stuff, fast stuff, heavy stuff, dark stuff, turbulence, and the concept of time."*
>
> — Zach Weinersmith, Science: Abridged Beyond the Point of Usefulness

We have not figured it all out and we may never will. But I believe we know enough. Although interesting, more research is *not* needed. What is desperately needed is decisive action against climate change and the ongoing violation of any and all planetary boundaries of the earth system as described in the introduction of this thesis. Micro- and nanoplastics check at least two of the nine planetary boundary threats – contributing to pollution by novel entities and atmospheric aerosol loading. Indirectly they also contribute to the boundaries of biodiversity loss and climate change itself. However, blindly banning plastic and replacing it with often far more energy- and water-consumptive paper or glass is not always the answer. The solution must lie in the reduction (but not substitution) of futile single-use packaging, an increase in recycling rates and well-managed plastic waste in comparison to non- or mismanaged plastic, as well as in an overall responsible and mindful handling of earth's resources and our environment. The time to act is now.

Bibliography

[1] C. B. Crawford and B. Quinn, *Microplastic Pollutants*, 1st ed. Elsevier, 2017.

[2] PlasticsEurope, "Plastics - the Facts 2019," 2019.

[3] "Plastic bag ban in Austria as from 2020," *Federal Ministry Republic of Austria - Agriculture, Regions and Tourism*, 2019. [Online]. Available: https://www.bmlrt.gv.at/english/environment/Wastemanagement/Plastic-bag-ban-in-Austria-as-from-2020.html. [Accessed: 17-Apr-2020].

[4] R. Dris, J. Gasperi, M. Saad, C. Mirande, and B. Tassin, "Synthetic fibers in atmospheric fallout: A source of microplastics in the environment?," *Mar. Pollut. Bull.*, vol. 104, no. 1–2, pp. 290–293, 2016.

[5] M. Bergmann, S. Mützel, S. Primpke, M. B. Tekman, J. Trachsel, and G. Gerdts, "White and wonderful? Microplastics prevail in snow from the Alps to the Arctic," *Sci. Adv.*, vol. 5, no. 8, pp. 1–11, 2019.

[6] L. Cai *et al.*, "Characteristic of microplastics in the atmospheric fallout from Dongguan city, China: preliminary research and first evidence," *Environ. Sci. Pollut. Res.*, vol. 24, no. 32, pp. 24928–24935, 2017.

[7] S. Allen *et al.*, "Atmospheric transport and deposition of microplastics in a remote mountain catchment," *Nat. Geosci.*, vol. 12, no. 5, pp. 339–344, 2019.

[8] M. Ganguly and P. A. Ariya, "Ice Nucleation of Model Nanoplastics and Microplastics: A Novel Synthetic Protocol and the Influence of Particle Capping at Diverse Atmospheric Environments," *ACS Earth Sp. Chem.*, vol. 3, no. 9, pp. 1729–1739, 2019.

[9] J. Rockström *et al.*, "A safe operation space for humanity," *Nature*, vol. 461, no. September, pp. 472–475, 2009.

[10] W. Steffen *et al.*, "Planetary boundaries: Guiding human development on a changing planet," *Science (80-.).*, vol. 347, no. 6223, 2015.

[11] G. A. Burton, "Stressor Exposures Determine Risk: So, Why Do Fellow Scientists Continue to Focus on Superficial Microplastics Risk?," *Environ. Sci. Technol.*, vol. 51, no. 23, pp. 13515–13516, 2017.

[12] O. Hollóczki and S. Gehrke, "Can Nanoplastics Alter Cell Membranes?," *ChemPhysChem*, pp. 9–12, 2019.

[13] J. A. Pitt *et al.*, “Uptake, tissue distribution, and toxicity of polystyrene nanoparticles in developing zebrafish (Danio rerio),” *Aquat. Toxicol.*, vol. 194, no. November 2017, pp. 185–194, 2018.

[14] R. Lehner, C. Weder, A. Petri-Fink, and B. Rothen-Rutishauser, “Emergence of Nanoplastic in the Environment and Possible Impact on Human Health,” *Environ. Sci. Technol.*, 2019.

[15] J. C. Prata, “Airborne microplastics: Consequences to human health?,” *Environ. Pollut.*, vol. 234, no. February, pp. 115–126, 2018.

[16] J. P. da Costa, “Micro- and nanoplastics in the environment: Research and policymaking,” *Curr. Opin. Environ. Sci. Heal.*, vol. 1, pp. 12–16, 2018.

[17] J. Gasperi *et al.*, “Microplastics in air: Are we breathing it in?,” *Curr. Opin. Environ. Sci. Heal.*, vol. 1, pp. 1–5, 2018.

[18] H. G. Scheibel and J. Porstendoerfer, “Generation of monodisperse Ag- and NaCl-aerosols with particle diameters between 2 and 300 nm,” *J. Aerosol Sci.*, vol. 14, no. 2, pp. 113–126, 1983.

[19] “Industrial Emissions - Environment - European Commission.” [Online]. Available: https://ec.europa.eu/environment/industry/stationary/index.htm. [Accessed: 08-Jul-2020].

[20] A. Shrivastava, “Introduction to Plastics Engineering,” *Introd. to Plast. Eng.*, pp. 1–16, 2018.

[21] B. Zhang *et al.*, “Morphological Changes of Isotactic Polypropylene Crystals Grown in Thin Films,” *Macromolecules*, vol. 50, no. 16, pp. 6210–6217, 2017.

[22] “Thermoplastic and Thermosetting Polymers | MATSE 81: Materials In Today’s World.” [Online]. Available: https://www.e-education.psu.edu/matse81/node/2209. [Accessed: 29-Jun-2020].

[23] X.-F. Wei, E. Linde, and M. S. Hedenqvist, “Plasticiser loss from plastic or rubber products through diffusion and evaporation,” *npj Mater. Degrad.*, vol. 3, no. 1, 2019.

[24] I. C. Mcneill, “Thermal Degradation,” in *Comprehensive Polymer Science and Supplements*, 2nd Editio., G. Allen and J. C. Bevington, Eds. Pergamon, 1996, pp. 451–500.

[25] D. M. Mitrano, “(Micro)Plastic : From Consumer Materials to the Environment,” in *Eawag: Swiss Federal Institute of Aquatic Science and Technology*.

[26] “Sigma-Aldrich.” [Online]. Available: https://www.sigmaaldrich.com/austria.html. [Accessed: 28-Jun-2020].

[27] J. Sun, X. Dai, Q. Wang, M. C. M. Van Loosdrecht, and B. Ni, “Microplastics in wastewater treatment plants : Detection , occurrence and removal,” *Water Res.*, vol. 152, pp. 21–37, 2019.

[28] A. Murray and B. Örmeci, “Removal effectiveness of nanoplastics (<400 nm) with separation processes used for water and wastewater treatment,” *Water (Switzerland)*, vol. 12, no. 3, 2020.

[29] P. He, L. Chen, L. Shao, H. Zhang, and F. Lu, “Municipal solid waste (MSW) landfill: a source of microplastics? -Evidence of microplastics in landfill leachate,” *Water Res.*, no. 159, pp. 38–45, 2019.

[30] Z. Yang, F. Lü, and W. Wang, “Is incineration the terminator of plastics and microplastics ?,” *J. Hazard. Mater.*, vol. 401, no. June 2020, p. 123429, 2021.

[31] C. M. Rochman and T. Hoellein, “The global odyssey of plastic pollution,” *Science*, vol. 368, no. 6496, pp. 1184–1185, 2020.

[32] S. Allen, D. Allen, K. Moss, G. Le Roux, V. R. Phoenix, and J. E. Sonke, “Examination of the ocean as a source for atmospheric microplastics,” *PLoS One*, vol. 15, no. 5, pp. 1–14, 2020.

[33] J. Gigault *et al.*, “Current opinion: What is a nanoplastic?,” *Environ. Pollut.*, vol. 235, pp. 1030–1034, 2018.

[34] J. P. da Costa, P. S. M. Santos, A. C. Duarte, and T. Rocha-Santos, “(Nano)plastics in the environment - Sources, fates and effects,” *Sci. Total Environ.*, vol. 566–567, pp. 15–26, 2016.

[35] Dalberg Advisors, W. de Wit, and N. Bigaud, “Assessing plastic ingestion from nature to people (AN ANALYSIS for WWF),” p. 7, 2019.

[36] X. Chang, Y. Xue, J. Li, L. Zou, and M. Tang, “Potential health impact of environmental micro- and nanoplastics pollution,” *J. Appl. Toxicol.*, vol. 40, no. 1, pp. 4–15, 2020.

[37] “Air pollution.” [Online]. Available: https://www.who.int/health-topics/air-pollution. [Accessed: 23-Jul-2020].

[38] W. C. Hinds, *Aerosol technology: properties, behavior, and measurement of airborne particles*. John Wiley & Sons, Incorporated, 1999.

[39] TSI Incorporated, “Fundamentals of Condensation Particle Counters (CPC) and Scanning Mobility Particle Sizer™ (Smps™) Spectrometers,” 2014.

[40] P. Kallinger, G. Steiner, and W. W. Szymanski, “Characterization of four different bipolar charging devices for nanoparticle charge conditioning,” *J. Nanoparticle Res.*, vol. 14, no. 6, 2012.

[41] G. Steiner, “High Resolution Mobility Spectrometry Of Molecular Ions And Their Effect On The Charging Probabilities Of Airborne Particles Under Bipolar Diffusion Charging Conditions,” University of Vienna, 2011.

[42] P. Intra and N. Tippayawong, “An overview of differential mobility analyzers for size classification of nanometer-sized aerosol particles,” *Songklanakarin J. Sci. Technol.*, no. 30 (2), pp. 243–256, 2008.

[43] “Development of new measurement methods for the characterization of nanometer-sized particles,” *University of Vienna - Aerosol Physics and Environmental Physics*. [Online]. Available: https://aerosols.univie.ac.at/research/development-of-new-measurement-methods-for-the-characterization-of-nanometer-sized-particles/. [Accessed: 24-May-2020].

[44] E. O. Knutson and K. T. Whitby, “Aerosol classification by electric mobility: apparatus, theory, and applications,” *J. Aerosol Sci.*, vol. 6, no. 6, pp. 443–451, 1975.

[45] R. C. Flagan, “On Differential Mobility Analyzer Resolution,” *Aerosol Sci. Technol.*, vol. 30, no. 6, pp. 556–570, 1999.

[46] “User’s Manual: Model 3068B Aerosol Electrometer,” *TSI Inc.*, 2009.

[47] “EMS-10 Control Center Operating Software EMSCC 1.4.” Tapcon & Analysesysteme GmbH, 2011.

[48] “Aerosol Instrument Manager ® Software,” *TSI Inc.*, 2010.

[49] M. Wojdyr, “Fityk.” 2016.

[50] “TSI Series 4000 / 4100 High Performance Linear OEM Mass Flowmeter,” *TSI Inc.*, 2004.

[51] S. Ray and R. P. Cooney, *Thermal degradation of polymer and polymer composites*, Third Edit. Elsevier Inc., 2018.

[52] “Jmol: an open-source java viewer for chemical structures in 3D.” .